UNIVERSIDADE FEDERAL DE SANTA CATARINA
CENTRO TECNOLÓGICO DE JOINVILLE
PROGRAMA DE PÓS-GRADUAÇÃO EM ENGENHARIA E CIÊNCIAS MECÂNICAS

Rodrigo Silveira de Santiago

NUMERICAL ANALYSIS OF MECHANICAL FATIGUE IN PLATE AND SHELL HEAT EXCHANGERS

Joinville
2021

Rodrigo Silveira de Santiago

NUMERICAL ANALYSIS OF MECHANICAL FATIGUE IN PLATE AND SHELL HEAT EXCHANGERS

Dissertação submetida ao Programa de Pós-Graduação em Engenharia e Ciências Mecânicas da Universidade Federal de Santa Catarina para a obtenção do título de Mestre em Engenharia e Ciências Mecânicas
Orientador: Profa. Talita Sauter Possamai, Dra.

Joinville
2021

Ficha de identificação da obra.

Silveira de Santiago, Rodrigo
Numerical Analysis of Mechanical Fatigue in Plate and Shell Heat Exchangers / Rodrigo Silveira de Santiago ; orientadora, Talita Sauter Possamai, 2021.
121 p.

Dissertação (mestrado) - Universidade Federal de Santa Catarina, Campus Joinville, Programa de Pós-Graduação em Engenharia e Ciências Mecânicas, Joinville, 2021.

Inclui referências.

1. Engenharia e Ciências Mecânicas. 2. PSHE. 3. FEA. 4. Fadiga. I. Sauter Possamai, Talita. II. Universidade Federal de Santa Catarina. Programa de Pós-Graduação em Engenharia e Ciências Mecânicas. III. Título.

Rodrigo Silveira de Santiago

NUMERICAL ANALYSIS OF MECHANICAL FATIGUE IN PLATE AND SHELL HEAT EXCHANGERS

O presente trabalho em nível de Mestrado foi avaliado e aprovado pela banca examinadora composta pelos seguintes membros:

Profa. Talita Sauter Possamai, Dra.
Universidade Federal de Santa Catarina

Prof. Kleber Vieira de Paiva, Dr.
Universidade Federal de Santa Catarina

Prof. Marcos Alves Rabelo, Dr.
Universidade Federal de Santa Catarina

Prof. Guilherme Rosa Franzini, Dr.
Escola Politécnica da Universidade de São Paulo

Certificamos que esta é a **versão original e final** do trabalho de conclusão que foi julgado adequado para obtenção do título de mestre em Engenharia e Ciências Mecânicas.

ICP-Edu
Documento assinado digitalmente
Rafael de Camargo Catapan
Data: 10/11/2021 13:46:05-0300
CPF: 029.036.159-18
Verifique as assinaturas em https://v.ufsc.br

Rafael de Camargo Catapan, Dr.
Coordenação do Programa de Pós-Graduação

ICP-Edu
Documento assinado digitalmente
Talita Sauter Possamai
Data: 10/11/2021 09:43:50-0300
CPF: 052.039.319-84
Verifique as assinaturas em https://v.ufsc.br

Profa. Talita Sauter Possamai, Dra.
Orientadora
Joinville, 2021.

AGRADECIMENTOS

Agradeço a Petrobras pelo suporte financeiro e apoio a pesquisa.

Agradeço a Profa. Talita Sauter Possamai pela orientação, apoio e pelo exemplo como professora e pesquisadora.

Ao professor Renato Oba por todas as contribuições no decorrer do trabalho.

Ao doutorando Giovani Martins por ter ajudado no desenvolvimento deste trabalho ao realizar a sua dissertação em paralelo. O trabalho em conjunto foi crucial para a obtenção dos resultados presentes neste documento.

Agradeço à UFSC, aos seus profissionais e colaboradores, pelas oportunidades oferecidas, em especial ao programa de pós Graduação em Engenharia e Ciências Mecânicas.

Agradeço aos professores participantes da banca pelas sugestões, críticas e contribuições finais que deram ao trabalho.

Agradeço ao Thermal Fluid Flow Group e todos os seus participantes pela disponibilização do equipamento e experiências que possibilitaram o desenvolvimento deste trabalho.

Agradeço também aos amigos que fiz no laboratório, Bruna, Vanessa e Arthur e por todo o tempo que dedicamos juntos.

Agradeço em especial a Damylle e ao Rafinha, por estarem ao meu lado sempre, e é claro a minha mãe e irmãos pelo apoio incondicional.

Viver é arriscar tudo. Caso contrário você é apenas um pedaço inerte de moléculas montadas aleatoriamente à deriva onde o universo te sopra. (Rick and Morty, 2017)

RESUMO

Trocadores de calor de placas são amplamente utilizados na indústria devido à sua versatilidade, flexibilidade de configuração geométrica e baixa razão entre a área de transferência de calor e o volume. Dentre os diversos modelos, os de placas são bastante utilizados na indústria de petróleo e gás. Devido à natureza do seu funcionamento, esses trocadores sofrem elevados gradientes térmicos e de pressão entre os bocais de entrada e saída, que ao longo do funcionamento do trocador, podem causar a falha por fadiga. Em especial, o Trocador de Calor de Casco e Placas (PSHE) tem a maior tendência de sofrer este efeito, visto que o processo de fabricação por soldagem para unir as placas pode induzir trincas, defeito crucial para a falha por fadiga. Neste trabalho, analisa-se numericamente o comportamento estrutural de um conjunto de 4 placas de trocadores de calor do tipo PSHE sofrendo carregamento de pressão estática e alternada, a fim de avaliar o comportamento estrutural e a vida em fadiga dos componentes por meio da análise de elementos finitos. Os resultados obtidos pelo modelo são comparados com testes experimentais obtidos da literatura para a mesma geometria e configuração demonstrando diferenças na tensão de von Mises em diferentes partes da placa abaixo de 20% A influência da modelagem da solda entre as placas no modelo numérico foi analisada indicando que devido à dificuldade em prever as propriedades da solda com precisão, o modelo numérico não consegue estimar a vida em fadiga com confiabilidade, sendo necessária a utilização de fatores de redução de vida em fadiga para todos os critérios de falha, concordando com os dados experimentais, apresentando desvios de no máximo 25%. Por fim foram analisadas numericamente as tensões ao longo do topo dos canais e a força de separação entre as placas centrais, indicando picos de tensão deslocados da linha central da corrugação na região de contato.

Palavras-chave: PSHE, FEA, Fadiga, Trocador de Calor.

RESUMO EXPANDIDO

Introdução

Trocadores de calor de placas são amplamente utilizados na indústria devido à sua versatilidade, flexibilidade de configuração geométrica e baixa razão entre a área de transferência de calor e o volume. Dentre os diversos modelos, os de placas são bastante utilizados na indústria de petróleo e gás. Devido à natureza do seu funcionamento, esses trocadores sofrem elevados gradientes térmicos e de pressão entre os bocais de entrada e saída, que ao longo do funcionamento do trocador, podem causar a falha por fadiga. Em especial, o Trocador de Calor de Casco e Placas (PSHE) tem a maior tendência de sofrer este efeito, visto que o processo de fabricação por soldagem para unir as placas pode induzir trincas, defeito crucial para a falha por fadiga. Neste trabalho, analisa-se numericamente o comportamento estrutural de placas de trocadores de calor do tipo PSHE sofrendo carregamento de pressão estática e alternada, a fim de avaliar o comportamento estrutural e a vida em fadiga dos componentes por meio da análise de elementos finitos (FEA).

Objetivos

O principal objetivo do trabalho é realizar a modelagem numérica e a análise de deformações mecânicas e vida à fadiga devido ao funcionamento de um Trocador de Calor de Casco e Placas (PSHE), com foco nas placas do trocador, usando um modelo simplificado de 4 placas. Os objetivos específicos são os seguintes: Apresentar o estado da arte dos trocadores de calor a placas no que diz respeito à análise de vida à fadiga e comportamento mecânico; modelar numericamente o comportamento mecânico de um PSHE; validar o modelo numérico com base em dados experimentais fornecidos pela literatura; realizar o estudo do comportamento do campo de tensões na região de contato das placas e da influência do dimensionamento da superfície da placa; por fim, analisar o comportamento da vida em fadiga e comparar com os resultados experimentais.

Metodologia

Apenas uma geometria de placa corrugada foi analisada, apresentando diâmetro externo de 310 mm, diâmetro dos bocais de 55 mm, distância entre bocais de 235 mm e ângulo de corrugação de 36,87°, feito a base de aço inoxidável 316L. Tendo em vista que existia uma grande quantidade de dados experimentais de trabalhos presentes na literatura para a mesma placa, viabilizando a validação do modelo, o modelo numérico buscou apresentar as condições de contorno mais próximas das utilizadas experimentalmente. Para isso foram utilizadas apenas 4 placas para modelar o conjunto de placas presentes no trocador, das quais apenas as internas (placas 2 e 3) não apresentavam comportamento de corpo rígido. Para as placas externas, foi a aplicada a condição de suporte fixo em todas as superfícies, impedindo que as placas externas percam o contato e emulando os pontos de contato entre as placas externas e internas.

Tendo em vista que o conjunto de placas do trocador de calor é unido por processo de soldagem, as soldas foram modeladas como um aro com seção quadrada, tanto para as soldas externas quanto para as internas. Duas configurações foram avaliadas nos modelos desenvolvidos: a solda constituída do mesmo material da placa, chamado material-base, e a solda constituída de um material semelhante ao de base, mas com propriedades mecânicas que simulam a modificação do efeito de soldagem, desprezando a zona termicamente afetada.

Para o carregamento de pressão hidrostática, foram realizados casos para ambas as configurações de propriedades de solda considerando a pressão entre as placas internas (2 e 3) de 0,8, 1,0, 1,2, 1,4 e 1,6 bar. Para os casos considerando o carregamento de pressão hidrostática em ambos os ramais, apenas a condição de 1,4 bar foi analisada.

Por último, foi realizada a análise numérica de vida em fadiga para os critérios de falha por fadiga de Gerber, Goodman e Soderberg. Tendo em vista os efeitos da solda em processos de fadiga, fez-se necessário utilizar fatores de redução de vida em fadiga. Neste caso, foram utilizados os fatores presentes na norma ASME, os utilizados por Martins (2019) nos testes experimentais e os fatores ideias para obter o mesmo número de ciclos de operação obtidos nos testes experimentais utilizando a abordagem numérica.

Resultados e Discussões

Foram obtidos os campos de tensão para todas as pressões apresentadas na metodologia e retirados os valores de tensão localizados nos mesmos pontos em que Martins (2019) posicionou os extensômetros. Observou-se comportamento praticamente linear da tensão em relação ao aumento da pressão. Foram também obtidos os valores de pico de tensão para a corrugação fora da região de contato, os bocais de entrada e saída e a região da solda externa, sendo esta última a que apresentou maiores valores de tensão.

O modelo com solda de mesmo material que o material-base das placas não ultrapassou 25% de erro para oito dos doze pontos comparados. O mesmo comportamento ocorreu para os testes com a solda considerando o material diferente, tendo este um erro máximo de 30% para tais pontos. Os pontos que apresentaram erro acima deste valor para ambos os casos, indicaram desvios de 80 a 90%.

Atribui-se a esses pontos principalmente o efeito de variações na geometria em relação à geometria real utilizada nos testes experimentais, principalmente em reforços localizados nesta região. Ao avaliar-se o campo de deslocamento ao longo da placa notaram-se picos de deslocamento na região correspondente aos pontos de maiores desvios de tensão, indicando a falta de precisão entre a geometria real e a numérica para esta região.

Para realizar os testes de vida em fadiga fez-se necessário utilizar o campo de tensão equivalente de von Mises das análises estáticas. Para as análises realizadas por Martins (2019), o ponto avaliado apresentou cerca de 80% de desvio no modelo numérico e este não estava localizado na região ao longo da solda externa (visto a dificuldade de se colocar um extensômetro em tal região). Tendo conhecimento disso, optou-se por utilizar a região de maior tensão ao longo da solda externa nas análises numéricas e comparar os resultados de vida em fadiga com os testes experimentais.

Apesar de este ponto não ser o mesmo dos testes experimentais, os desvios do pico de tensão da solda para o modelo numérico não foram superiores a 20%. Foram realizados testes utilizando os critérios de falha de vida em fadiga de Gerber, Sodeberg e Goodman e variando os valores do fator de correção de vida em fadiga entre 1 e 6,2 - sendo que os valores acima de 4 não são estipulados por norma.

Percebeu-se que, para todos os critérios de falha e valores abaixo de 3 no fator de redução de vida em fadiga, a vida foi superestimada em relação aos testes experimentais. Valores superiores a 4 apresentaram vida próxima à encontrada para valores experimentais, levando em consideração o quão conservador o critério de falha era e o quão alto era o fator de redução de vida em fadiga utilizado.

É importante ressaltar que, indiferentemente da variação de propriedade mecânica da solda, a número de ciclos obtidos entre os dois modelos de análise fora similar, visto que o valor de pico de tensão entre ambos não era superior a 3,5%. Dos três critérios de falha utilizados, os critérios de Goodman e Gerber apresentaram as melhores aproximações do comportamento de vida em fadiga na região da solda, utilizando os fatores de redução de vida em fadiga de 4,5 e 5, respectivamente.

Um ponto de contato arbitrário foi estudado de forma mais localizada para as pressões de 1 e 1,4 bar de forma a entender o comportamento do campo de tensão na região de contato.

Observaram-se três picos de tensão ao longo da área do ponto de contato: um de maior intensidade e dois secundários. Este pico de tensão principal ultrapassou a tensão de escoamento do material indicando que na área de contato entre as placas ocorre deformação plástica. Apesar disso, é notável indicar que essa região corresponde a uma parcela muito pequena da área de contato.
Para tentar entender o comportamento de tensão ao longo da placa, foram obtidos valores de tensão equivalente de von Mises ao longo do topo da corrugação de diferentes linhas em zig-zag: próximo do bocal de entrada, no centro da placa e perto do bocal de saída. Esta análise levou à conclusão de que os valores não ultrapassaram os limites de escoamento do material, indicando que o pico de tensão observado na análise anterior se encontra levemente defasado em relação à linha central da corrugação. Observou-se também que ao se aproximar da região dos Vs ao longo do zig-zag, o nível de tensão aumenta abruptamente, variando de 50 a 150MPa. Isto indica que a força de contato ao longo dos pontos de contato na corrugação dependem do ângulo de Chevron e que a força não é uniformemente distribuída ao longo da área de contato.
Por fim, realizou-se a análise do efeito dos carregamentos entre placas internas, externas e o carregamento simultâneo. Observou-se que quando aplicado um carregamento de pressão hidrostática em apenas um dos ramais, seja interno ou externo, há um aumento drástico na tensão da região de contato, provocando a deformação plástica da região. O mesmo não ocorre quando o carregamento é aplicado em ambos os ramais, visto que as pressões são aplicadas em ambos os lados da placa e tendem a ter o seu efeito reduzido, diminuindo os picos de tensão nos pontos de contato, bem como a tensão ao longo de toda a corrugação.

Conclusões

A modelagem numérica desenvolvida no presente trabalho possibilitou obter o estado de tensão ao longo das placas de um trocador de calor, identificando que, apesar de as tensões nos pontos de contato e ao longo da região da solda serem elevadas, a maior parte da corrugação sequer atinge valores próximos do limite de escoamento do material de base. A utilização de propriedades mecânicas diferentes para a solda não levou a variações significativas de tensão para os pontos medidos.
A metodologia utilizada para avaliar a vida em fadiga se mostrou válida para estimar o número de ciclos necessários para a falha e o processo de fadiga mostrou-se dependente do critério de falha utilizado e dos fatores de redução de vida em fadiga.

Palavras-chave: PSHE, FEA, Fadiga, Trocador de Calor.

ABSTRACT

Plate heat exchangers are widely used in industry due to their versatility, geometric configuration flexibility, and low heat transfer area-to-volume ratio. Among the various models, the plate ones are widely used in the oil and gas industry. Due to the nature of their operation, these exchangers suffer high thermal and pressure gradients between the inlet and outlet nozzles, which during the operation of the exchanger, can cause fatigue failure. In particular, the Plate and Shell Heat Exchanger (PSHE) has the greatest tendency to suffer this effect as the welding fabrication process to join the plates can induce cracks, a defect that is crucial for fatigue failure. In this work, the structural behavior of PSHE-type heat exchanger plates under static and alternating pressure loading is analyzed, in order to evaluate the structural behavior and fatigue life of the components through finite element analysis. The results obtained by the model are compared with experimental tests obtained from the literature for the same geometry and configuration demonstrating differences in the von Mises stress in different parts of the plate below 20%. that due to the difficulty in predicting the weld properties accurately, the numerical model cannot reliably estimate fatigue life, requiring the use of fatigue life reduction factors for all failure criteria, agreeing with experimental data, with deviations of at most 25%. Finally, the stresses along the top of the channels and the separation force between the central plates were numerically analyzed, indicating stress peaks displaced from the central line of the corrugation in the contact region.

Keywords: PSHE, FEA, Fatigue, Heat Exchanger

LIST OF FIGURES

LIST OF TABLES

LIST OF ABREVIATIONS AND ACRONYMS

GPHE Gasketed Plate Heat Exchanger

PSHE Plate and Shell Heat Exchanger

PCHE Printed Circuit Heat Exchanger

STHE Shell and Tube Heat Exchanger

PFHE Plate and Fin Heat Exchanger

FEM Finite Element Method

UTS Ultimate Tensile Strength

YS Yield Strength

LIST OF SYMBOLS

β	Chevron Angle	[°]
D_p	Diameter of inlet and outlet ports	[m]
L_d	Plate's diameter	[m]
L_b	Distance between inlet and outlet ports centers	[m]
S	Fatigue resistance	[MPa]
N	Number of cycles	[-]
a,b	Boundary condition's constants	[-]
E	Young's Module	[GPa]
S_y	Yield Strength	[MPa]
S_{ut}	Ultimate Tensile Strength	[MPa]
S_m	Fatigue resistance at 10^3 cycles	[-]
S_e	Fatigue resistance at 10^6 cycles	[-]
σ	Stress	[MPa]
σ_a	Alternated stress	[MPa]
σ_m	Mean stress	[MPa]
δ	Strain	[mm/mm]

SUMÁRIO

1 INTRODUCTION

Heat exchangers are equipment widely used in the petrochemical, textile, food and transportation industries as they allow heat transfer between two or more fluids with different temperatures. Their use are very varied, with specific configurations for each application. These configurations can be classified based on the process of thermal exchange, use of regenerators, constructive type (tubes, plates and shells) and others.

During operation, the heat exchanger may be subjected to high thermal and pressure gradients between the inlet and outlet of the working fluids, increasing the possibility of fatigue after a certain number of life cycles. Adolfsson and Rashid (2016) estimate that plate heat exchangers operate for 70% of the year, with preventive maintenance, failures or cleaning as the main causes of stoppage. Over 30 years, it is estimated that for a plate heat exchanger the total cost associated with maintenance is about 32% of the total cost of operation.

In the case of Gasketed Plate Heat Exchanger (GPHE), the gasket may break or slip from its position, causing damage to the process and equipment. Unlike GPHEs, Plate and Shell Heat Exchanger (PSHE) are sealed using brazing or welding process. This allows less leakage in the joint between the plates and greater operating pressures. On the other hand, the bonding process can induce cracks and pores in the material, reducing the life of the exchanger in this region, in addition to making it difficult to clean the equipment (LI et al, 2019).

In this work it is proposed to study Plate and Shell Heat Exchangers (PSHEs) using the Finite Element Method (FEM) to analyze the stresses and displacements caused by the operation under various conditions.

1.1 OBJECTIVES

1.1.1 Main Objective

Numerical modeling and analysis of mechanical strains and fatigue life due to the operation of a Plate and Shell Heat Exchanger (PSHE), focusing on the exchanger plates, using a simplified 4-plate model.

1.1.2 Specific Objectives

- Present the state of the art of plate heat exchangers regarding the analysis of fatigue life and mechanical behavior;
- Numerically model the mechanical behavior of a 4-plate set of a PSHE ;
- Validate the numerical model based on experimental data provided by the literature;
- Study the behavior of the stress field in the contact region of the plates and the influence of the plate surface design;
- Analyze fatigue life behavior and compare with experimental results.

1.2 JUSTIFICATION

Currently, in the literature the number of studies focused on plate heat exchangers related to fatigue life analysis is scarce, regardless of the geometry. The approach by numerical simulation in PHEs, shows a certain lack in relation to the mapping of stress fields (influence of thermal and mechanical loads). A more detailed assessment of structural behavior in PHEs is the most significant contribution provided by this study.

2 BASIC CONCEPTS AND BIBLIOGRAPHIC REVIEW

2.1 COMPACT HEAT EXCHANGERS

Plate Heat Exchangers (PHEs) are manufactured using stacked plate sets. The exchanger channels are formed from the overlap of the different corrugated plates, with the passage of fluid in the gaps between the plates. These plates have great flexibility as to the cross-section's geometry of the corrugation, admitting channels with semicircular of sinusoidal geometries and Chevron[1] angles. The latter on of the most employed configurations. Figure 1 illustrates a Gasketed Plate Heat Exchanger (GPHE). On the left is possible to visualize the gasket over one plate while on the right a full gasketed plate heat exchanger with a pack of more than 100 plates is shown. The yellow plastic indicates the orifices for the inlet and outlet flow of fluids.

Figure 1 – Gasketed Plate Heat Exchanger. Left: front view of a plate with the gasket. Right: a mounted gasketed plate heat exchanger.

Source: Author (2021)

[1] Chevron angle is the angle formed by the overlap of the channels of a pair of the exchanger's plates.

The geometry arrangements of the cross section and direction of the channel allows to increase the ratio between the useful heat transfer area and the occupied volume. This allows the exchanger to have higher convection heat transfer coefficients, since the geometry of the exchanger hinders flow development. This also results in greater friction factors and, consequently, in increased pressure drop between the inlet and outlet ports of the exchanger, having direct influence on the structural integrity of the equipment. In the case of gasketed exchangers, the operating limit is defined by the gasket material and geometry, which is restricted to temperature values between 40 and 180°C and pressure between 25 and 30 bar (KAKAÇ; LIU; PRAMUANJAROENKIJ, 2012).

An alternative to eliminate gasket-related problems is the Plate and Shell Heat Exchanger (PSHE) (see Figure 2). Unlike gasketed exchangers, plate and shell exchangers are sealed using welding or brazing process. This allows for greater joint strength, allowing the exchanger to operate at pressures up to 170 bar. As a major disadvantage, the cleaning process can only be done chemically, since the seal is permanent.

Figure 2 – Plate and Shell Heat Exchanger.

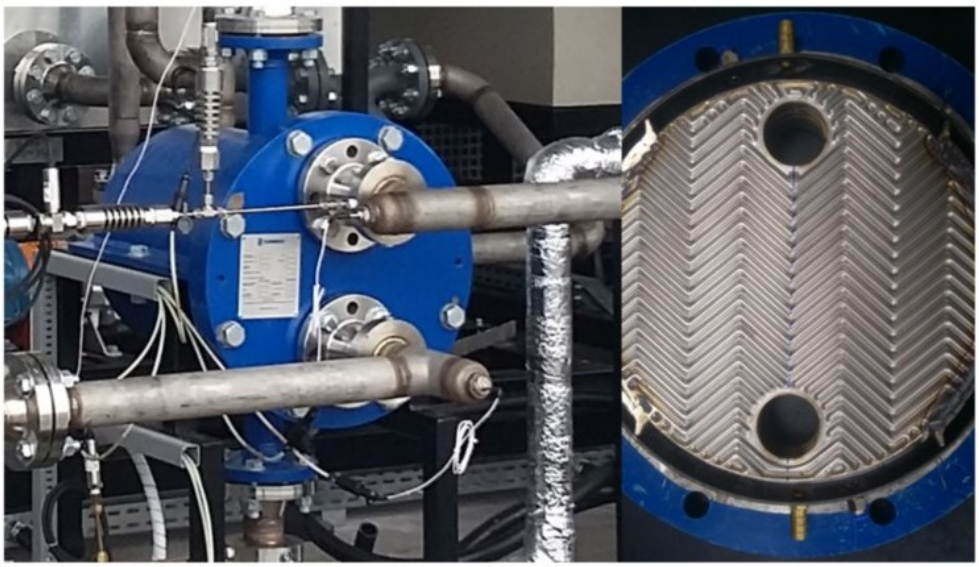

Source: Author (2021)

Although GPHEs do not support pressures as high as Shell and Tube Heat Exchangers (STHE), they have a high area density[2], reducing the difficulty of handling, cleaning and

[2] Area density is the ratio between the effective heat transfer area and the volume occupied by the heat exchanger.

maintenance, without suffering large losses in performance. Another exchanger with high area density is the so-called Printed Circuit Heat Exchanger (PCHE), shown in Figure 3, which can withstand pressures up to 500 bar and temperatures between -150°C and 700°C (THULUKKANAM, 2013). Table 1 presents the performance limits and characteristic dimensions of different exchangers according to the literature.

Figure 3 – Core of a Printed Circuit Heat Exchanger.

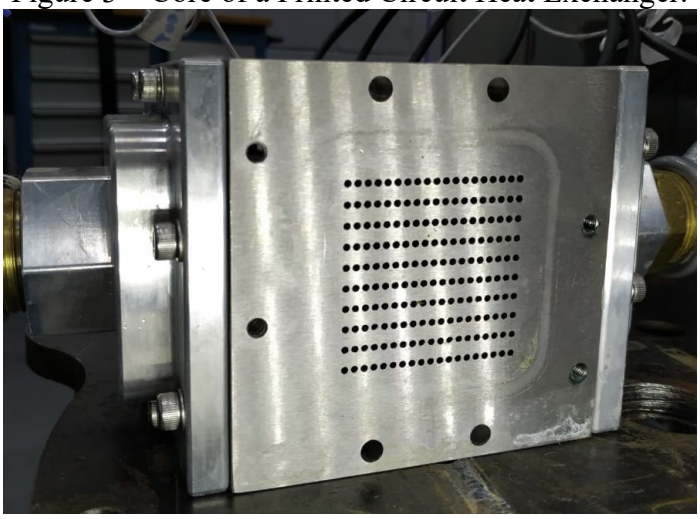

Source: Author (2021)

Table 1 – Performance limits and characteristic dimensions of different heat exchangers.

Type	ID	Area Density (mm^2/mm^3)	Maximum and minimum Temperatures (°C)	Maximum Operating Pressure (bar)
Shell and Tube	STHE	≤400	-20 to 500	600
Printed Circuit	PCHE	≥700	-150 to 700	500
Shell and Plate	PSHE	≥700	-80 to 890	170
Gasketed Plate	GPHE	≥700	40 to 180	30

Source: Adapted from Kakaç, Liu and Pramuanjaroenkij (2012) and Thulukkanam (2013)

Notice that the PSHE can withstand higher temperature and pressure than the GPHE, as commented before for the same order of area density, that are almost twice higher than the area density for the Shell and Tube heat exchanger.

2.1.1 Geometric Characteristics of the Analyzed Heat Exchanger

In plate heat exchangers with Chevron angle, the plates have corrugations with an angle (β) with the horizontal or vertical (depending on the reference), and the plates are mounted on top of each other rotating each plate 180°. Figure 4 shows the geometry of the shell and plate heat exchanger. The diameter of the entry and exit ports are given by D_p, L_d is the diameter of the plate and L_b is the distance between inlet and outlet ports centers. The Chevron angle is identified in Figure 4 by β.

The pairs of plates are initially welded on the outer perimeter and subsequently welded to the inlet and outlet ports of each pair, forming the pack of plates. Lids are then added to the last plate ports, to prevent the fluid passing through the pack from mixing with that passing through the shell. It is important to note that the working fluids, represented by the colors blue and red, do not mix within a pair of plates.

Different corrugation shapes can be found commercially. The corrugation shape studied in this work is presented in more details in Chapter 4.

Figure 4 – Geometry of a Plate and Shell Heat Exchanger. (a) Plate dimensions. (b) Flow direction.

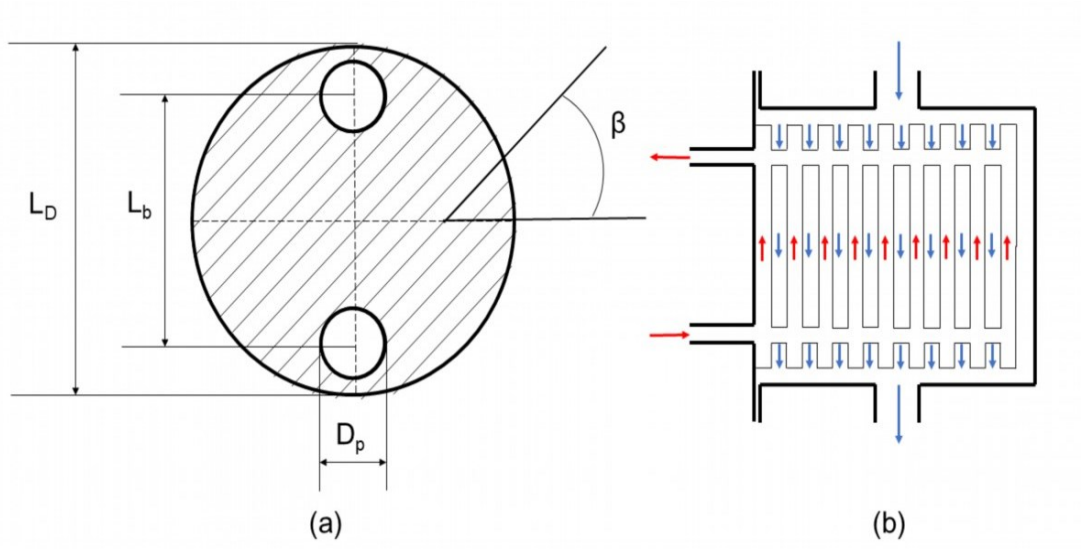

Source: Author (2021)

2.2 LITERATURE REVIEW

The literature on numerical and experimental studies related to the structural analysis of plate heat exchangers is scarce while several studies address the thermal fluid dynamic behavior of PHEs with the development of correlations for friction factor and Nusselt number[3]. In order to have a better understanding of this type of analysis in compact heat exchangers, the review below presents studies related to structural analysis of different types of compact heat exchangers, not limited to PHEs or PSHE.

2.2.1 Structural Analysis in Heat Exchangers

Song (2011) numerically analyzed a PCHE (Figure 5) with straight channels for high temperature applications (950°C). The thermal loading was obtained through simulations by finite differences along the exchanger to obtain the temperature profile. Prescribed pressure loading was imposed on the channel surfaces. The exchanger and the cold channel ports were produced in 316L stainless steel while the hot channel ports were produced in Inconel 800HT. The lower and upper covers of the exchanger were produced in 304 stainless steel. The mechanical properties of the material are shown by Song and Hong (2013) for the same exchanger.

Figure 5 – Numerical model of a PCHE.

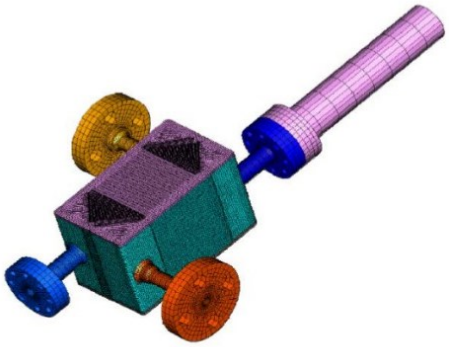

Source: Song (2011)

[3] Dimensionless number obtained from experimental data used to estimate the convection heat transfer coefficient

The temperature distribution along the channels was estimated from simulations using the I-DEAS/ TMG and ABAQUS software using SO_3 and H_2 as working fluids, with the hot channel operating between 770 and 850°C, and the cold channel between 450 and 750°C. Results showed that for high temperature gradients the thermal stress may be more significant for component failure. No experimental tests were performed to validate the stress field in the exchanger, nor were the dimensions of the exchanger informed.

Song, Hong and Park (2012) employed the same approach as Song (2011) to verify the influence of the mechanical properties variation of the material due to the increase in temperature. In addition, the average mechanical properties in the regions of addition material and thermally affected zone along the weld were evaluated. Add to this, the geometry of the exchanger, welds made with the tungsten inert gas process (TIG) to allow the channels to join were also considered in the model, including the melt pool along the edges of the exchanger and the thermally affected zone.

The thermal load was used as a load for the structural analysis, for operating condition of 850 ° C for the hot channel and 500 ° C for the cold channel. In this case the pressure loading was neglected. Elastic supports were used as a boundary condition for the fluid inlet and outlet ducts. For this purpose, the stiffness of the inlet and outlet ducts of the exchanger were calculated. The condition of contact with friction was imposed on the lower surface of the exchanger, with a friction factor of 0.1. Along this surface, a bulkhead was modeled to prevent deformation in this direction. The maximum stress value found in the stress field occurs near the elastic support region (310 MPa), exceeding the yield limit value for the alloy (233.5 MPa) for the temperature of 767 ° C. In the weld region, the maximum stress found is 273 MPa, exceeding the weld's Yield limit value by 1%. As this region is actually chamfered, something that was not designed in geometry, the maximum local stress found in the weld will reduce. Experimental tests were not used to validate the numerical model.

Song and Hong (2013) analyzed a 316L stainless steel PCHE for nuclear applications through numerical analysis. The model was developed in ABAQUS, in which simulations of heat exchange by conduction in the solid were initially carried out to obtain the temperature field along the exchanger. The temperature field was later validated using an infrared thermometer on an experimental bench (Figure 6). Subsequently, the temperature loading was used as a boundary condition for the structural tests. For the study, mechanical and thermal properties of the material were evaluated between 20 and 700 ° C.

Figure 6 – PCHE. (a) Experimental Setup. (b) Numerical Model.

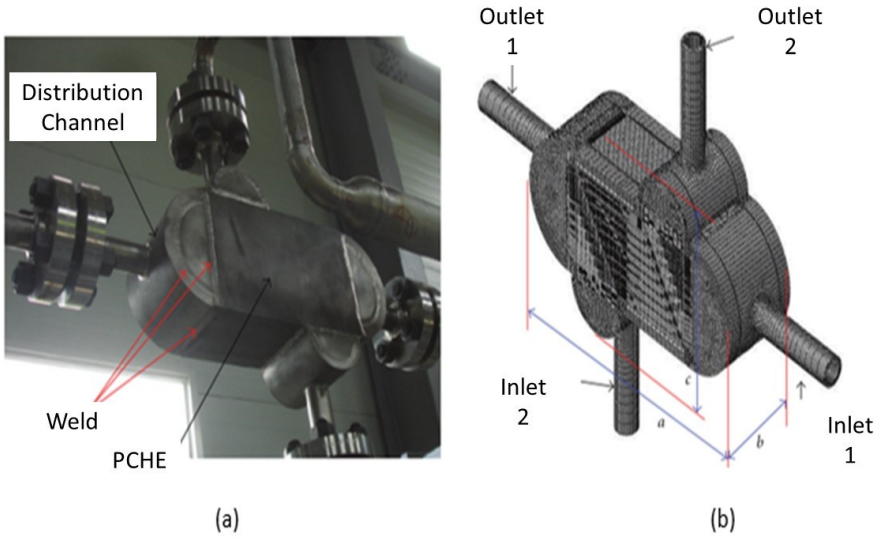

Source: Adapted from Song and Hong (2013)

Table 2 shows the properties of 316L Steel. In order to verify the effect of the welding process on the mechanical properties of the material, metallographies were performed on two samples in order to obtain the size of the weld bead and the thermally affected zone, in addition to induction tests to obtain Ultimate Tensile Strength (UTS) and Yield Strength (YS).

Table 2 - Properties of 316L Steel varying with temperature.

Temperature	**Young's Module**	**Poisson Coefficient**	**Thermal Conductivity**	**Specific Heat**	**Thermal Expansivity Coefficient**
(°C)	**(GPa)**	**(-)**	**(W/m°C)**	**(J/kgK)**	**(10^{-6}/°C)**
20	192	0.3	13.94	470	15.9
100	186	0.3	15.08	486	16.4
200	178	0.3	16.52	508	17
300	170	0.3	17.95	529	17.5
400	161	0.3	19.39	550	17.9
500	153	0.3	20.82	571	18.3
600	145	0.3	22.25	592	18.7
700	137	0.3	23.69	613	19.0

Source: Adapted from Song and Hong (2013).

For mechanical loading, the hot and cold channels were at 6 and 4 MPa, respectively. The elastic support model was used to model the support at the entrance and exit ports of the channels. It was observed that the highest stress concentration occurred at the edges of the weld.

Lee and Lee (2014) analyzed the influence of plasticity models for structural simulations in semi-circular channel PCHE with zigzag pattern (Figure 7). In the study, 2D cases of PCHE unit cells made with SS316 steel (with 2x1, 4x4 and 8x8 channel configuration) were compared, where initially the temperature profile along the exchanger geometry was obtained using the ANSYS Fluent software and later, for pressure loading, the pressure condition prescribed along the surface of the channels was used. These loads were introduced in ANSYS Mechanical in order to obtain the stress field in the geometry of the exchanger. No experimental tests were performed in the study. Properties such as modulus of elasticity and thermal expansion were analyzed between 482.2 and 593.3 ° C in order to verify the influence of thermal loading on the mechanical properties of the material. For the study, variations in the stress field in the preferred direction of flow in the channels were disregarded.

The elastic linear model diverges in crack nucleation regions, obtaining stress values tending to infinity, as for example at the tip of the channel, which in reality does not occur, since the process of joining by diffusion causes a rounding of the tip of the channel and the plastic strain that occur in this region cause a decrease in the level of stresses. To avoid unreal results, the tip of the channel has been rounded.

Figure 7 – PCHE with zig-zag channels.

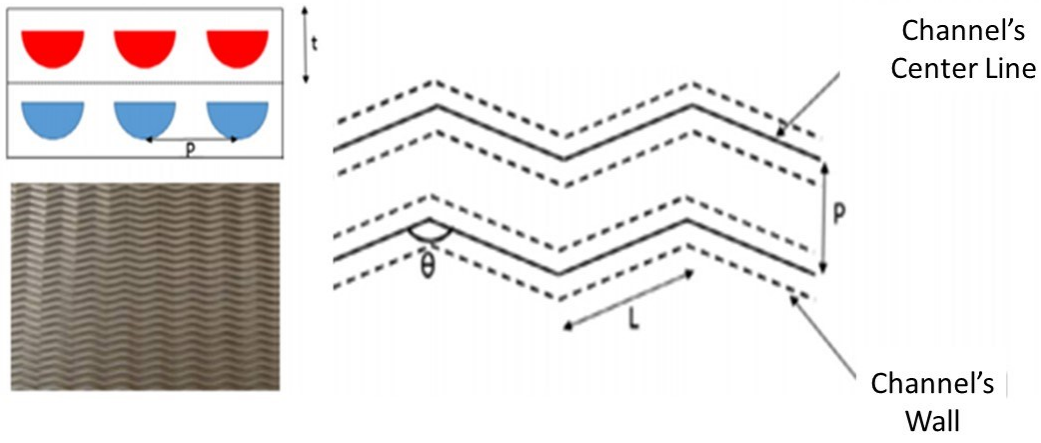

Source: Adapted from Lee and Lee (2014)

From the thermal loading, it can be observed that the temperature gradient in the transverse direction to the hot and cold channels is much higher than that found parallel to the

port axis, indicating that in this region there must be a higher stress concentration between the channels. The level of stress found around the cold channel is higher, mainly due to the high pressure in this channel. Due to the condition of symmetry used in the 2x1 model, the difference in the stress field is clear when compared with the 4x4 and 8x8 cases, which showed better coherence in the results. For most of the exchanger geometry, with the exception of the edges, the 4x4 model is able to represent the stress field, being the minimum configuration necessary for such a study.

When analyzing the pressure loading isolated, it can be seen that it has a greater influence on the concentration of stress at the edge of the channel, with the stress field not being uniformly distributed, having higher values around the cold channels. In the hot channels the intensity of the thermal stress and pressure is the same, while for the cold channel the high pressure of the channel is the factor with the greatest risk to the integrity of the exchanger, since the mechanical stress is much higher for this specific case.

To take into account the plasticity effect, the nonlinear stress-strain behavior model was used, in which the linear elasticity model for SS316 steel is evaluated at 510 ° C with the plasticity energy law model, allowing to obtain a non-linear curve relating stress and strain, which was later inserted in the bilinear isotropic model of plasticity to the hardening present in ANSYS. As a result, there is a reduction in the stress found at the end of the cold channel. Even if the stress reduction occurs at the tip of the channel, the model does not change the overall stress state, indicating that plastic strain only occurs in this region. The difference when using the plasticity model can be seen in Figure 8. The peaks in blue represent the stress that is poorly estimated due to the lack of a plasticity model.

Figure 8 – Comparison between the elastic linear model and the plasticity model.

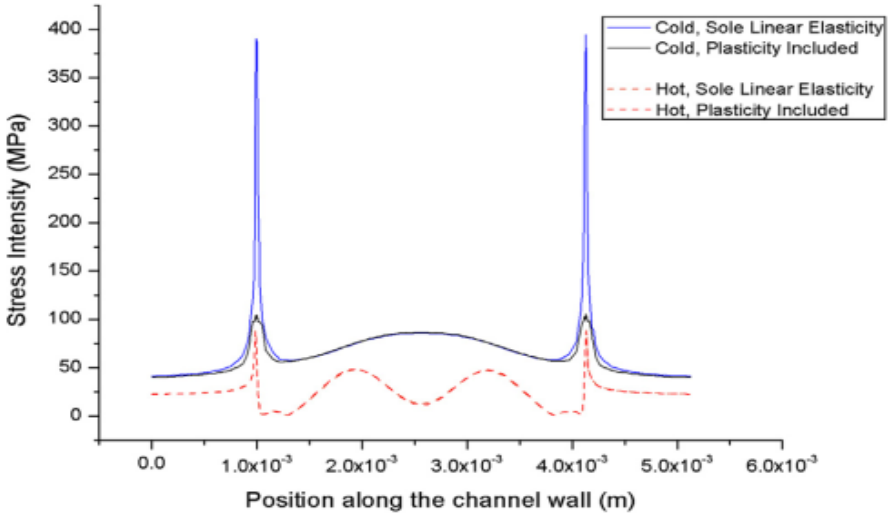

Source: Lee and Lee (2014)

Nascimento (2013) studied analytical models and numerical structural simulations to verify the failure of gasketed PHEs applied in the oil and gas industry. The heat exchanger plates are made of SB-2g5 Gr.1 Titanium alloy and the gasket consists of hydrogenated nitrile rubber (HNBR).

The first model used in the study consists of a one-dimensional analytical model that seeks to identify the main variables that influence sealing in addition to the theoretical pressure of separation between plates. For that, it was assumed that the joints and metallic contacts have the behavior of linear stiffness, the plates have medium displacement along the plane, and do not lose contact. Also the external plates have zero displacement, and the contact between the plates is evenly distributed over its surface. In the model, the behavior becomes critical when one of the compressive forces between the plates becomes null, causing the plates to separate the greater the initial clamping force, the greater the pressure required to leak.

The second model consists of a two-dimensional analysis by expanding Fourier series to estimate the displacement field, taking into account contact forces and the effect of contact points between plates. For that, the classic theory of plate bending was used and simplifications such as the approximation of the plate geometry to a smooth plate, contact points between plates with zero displacement, boundary condition for the periphery of the plates modeled as simple support (restricting only the linear displacements, but not rotational displacement) and geometry of the plate approximated by rectangular geometry. The model developed with MATLAB showed variations of 1.3% when compared to simulations of the same problem using

finite elements, but with a much higher computational cost, since for the case it was necessary to use 50 terms in each Fourier series. This modeling proved to be valid for plates with small amplitude corrugations where the rigidity and isotropy of the material are not altered by the corrugation and only in regions away from the edges of the plates, where the condition of simple support has an influence on the results. Figure 9 shows the displacement field found by both methods. In both cases, the hypothesis of null displacement at the contact points can be observed, while the rest of the plate presents an average displacement behavior.

Figure 9 – Displacement field. (a) Results obtained with the program developed in MATLAB. (b) Results obtained by FEM.

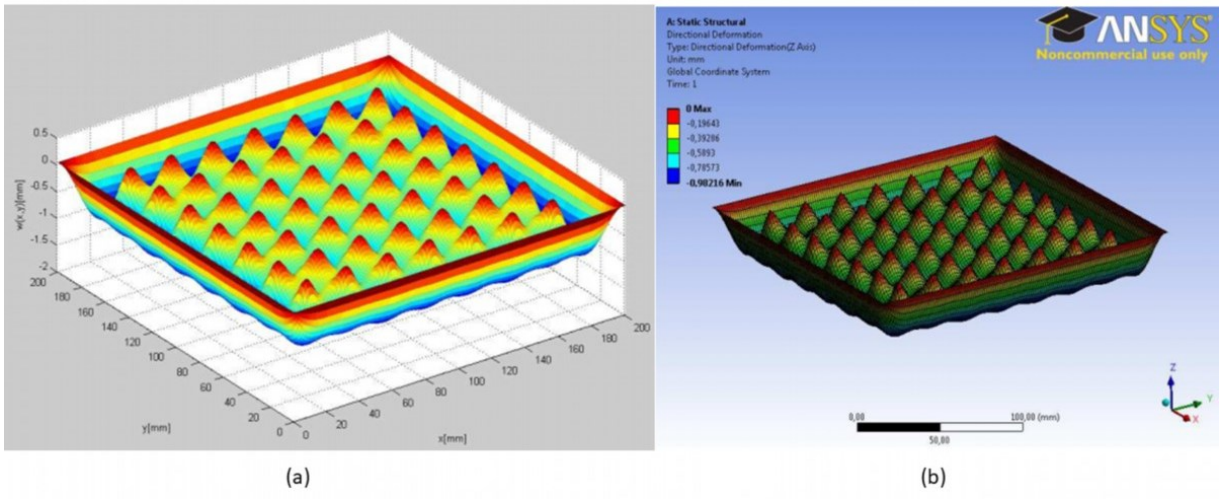

Source: Nascimento (2013)

Finally, a three-dimensional model was built considering only one sector of the corrugated plate, containing the channel to support the gasket. This geometry was later replicated 4 times and rotated to obtain the pack of 4 plates. Shell elements were used on the average surface of the plate thickness, allowing the calculation of membrane and bending stresses acting on the plate. The outer plates in the model are rigid and serve only to represent the clamping effect of the plates, compressing the internal (flexible) plates by 0.01 mm above and below. This tightening was used to guarantee contact between the plates, but without any effect of stresses caused by the closing. This configuration can be seen in Figure 10.

Subsequently, the pressure condition was applied to the outer surface of the internal plates with a value of 1 MPa, increasing their compression. The contact between the plates was modeled as Rough, preventing the tangential sliding of the plates, occurring only if the reaction on the surface is compressive, ensuring contact. To simplify the effect of the gaskets, the

condition of linear elastic support with stiffness of 4.1 N / mm³[4]was used. Finally, the hydrostatic pressure condition was applied to the internal surfaces of the internal plates. Lateral pressurization of the gasket was not considered.

The first result obtained was for the region of the elastic bases, allowing to evaluate the level of residual stress acting on the joint after pressurization considering that the joint has an initial compression of 1 MPa. This value was used to evaluate the previous compression of the joint due to the assembly being stipulated by the ASME BPVC Sec. VIII Div.1 standard.

As shown in Figure 10(b) the pressurization of the plates had little effect on the elastic bases, reaching the maximum value of 1 MPa for the region. This behavior is already expected since the initial compression value on the gasket was enough to prevent leakage and for smaller values, the failure could occur. It is important to note that this behavior is only valid because the joint has a square cross section.

Figure 10 – Numerical Model to evaluate the gasket region. (a) Configuration of the plates in the model. (b) Stress field in the gasket channel.

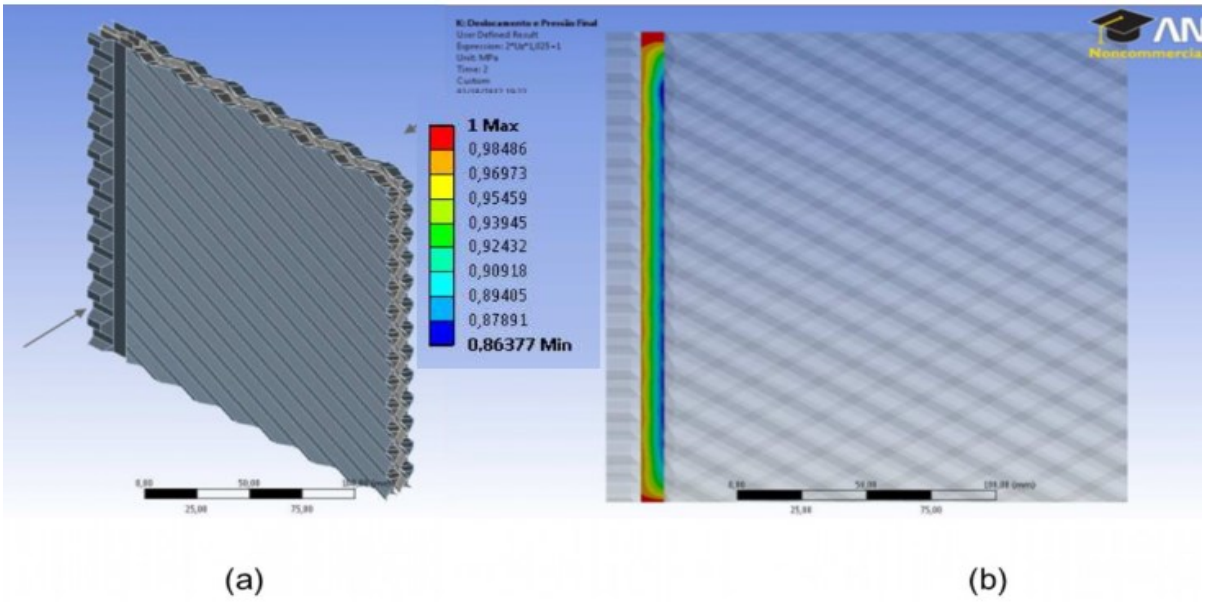

Source: Adapted from Nascimento (2013)

The results obtained with the analytical models were compared with numerical cases using the ANSYS program. For this, part of the geometry of the corrugated plate was modeled through a surface containing the gasket channel and heat exchange region. For the boundary conditions, simple supports were used along the perimeter of the plate, and on the central plates

[4] Spring stiffness per unit area

a pressure of 1 MPa was applied. As the friction coefficient between the plates is unknown, the contact condition between the plates was modeled as rough (“Rough”). On the external plates, the condition of average displacement of 0.1 mm was applied in order to compress the central plates and take into account the initial compression force on the plates.

Finally, a model was built to assess the stress level on the plate. For this, the same configurations between plates and boundary conditions that were used in Figure 10(a) were adopted, excluding only the region of the gasket channels to represent a central region of the plate. In Figure 11 , the single average displacement pattern can be observed, showing that the hypothesis adopted for the smooth plate model and the one-dimensional model is valid. In addition, the hypothesis of null displacement at the contact points is also valid, since the displacements in this region are much lower than those found in other regions, indicating the validity of the previously used two-dimensional model, given its restrictions. For the stress field (Figure 12), it was observed that for the central region of the plate, the contact points showed a higher stress value (about 100 MPa), exceeding the yield limit of the material.

Figure 11 – Displacement field obtained by the 3D model.

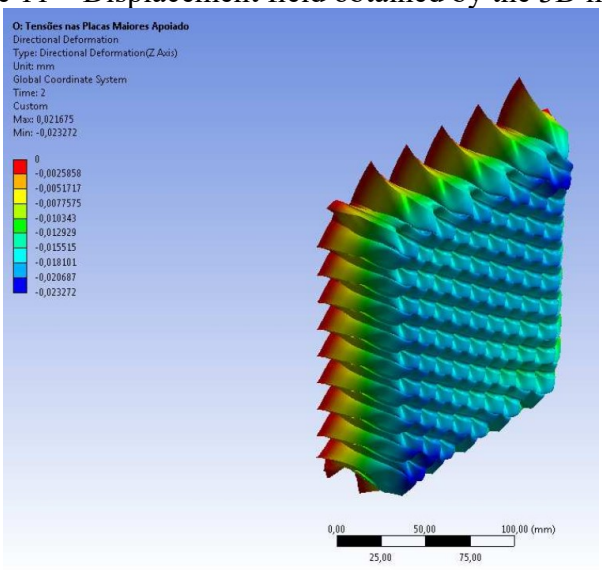

Source: Nascimento (2013)

Figure 12 – Stress field obtained by the 3D model.

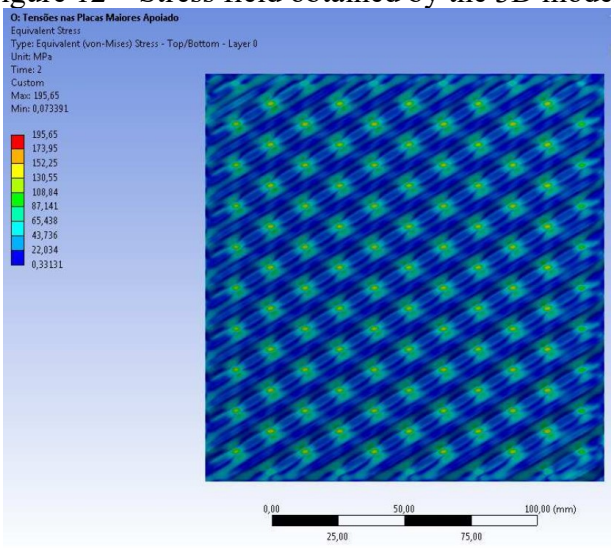

Source: Nascimento (2013)

Zhang et al (2015) analyzed numerically and experimentally plate and fin heat exchangers (PFHE), initially seeking to compare the thermo-hydrodynamic behavior of the exchanger with experimental tests and later verifying the influence of pressure distribution and temperature gradient of the surfaces with structural fluid interaction in the exchanger using the ANSYS software. In the study, oil and air were used as working fluids, where the oil was kept at a constant flow rate of 5.4 m^3/h, while the air flow rate was varied to obtain Reynolds values between 500 and 1500. Six geometries were modeled, varying dimensions of the fins and raised pressure drop curves, outlet temperature, convection coefficient and aspect ratio of the channels as a function of the Reynolds number. When comparing the pressure and temperature measurements between the experimental and numerical tests, deviations of 5% were found.

The results for structural fluid analysis showed maximum stress values located at the beginning and end of the fins, close to the welds. That same region is subject to variable loads due to flow, so it can easily suffer from fatigue failure. When assessing the effect of increasing the number of Reynolds on the maximum stress value (Figure 13), a slight drop in stress values is observed, while reducing the thickness causes an increase in maximum stress. To increase the distance between fins, the same behavior can be observed, with an increase in mechanical and thermal stresses.

Figure 13 – Stress variation with increasing number o Reynolds. (a) Decrease of the fin thickness. (b) Increased space between fins.

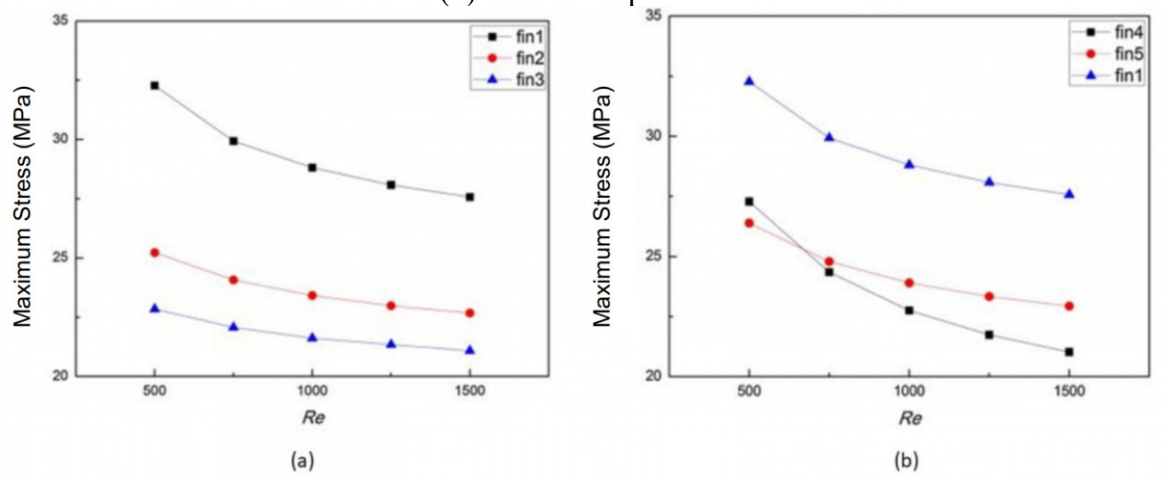

Source: Zhang et al (2015)

Zhang et al (2015) studied PCHEs with S-shaped fin channels for nuclear applications using the ANSYS software. This type of geometry appears as an alternative to the straight channel, zigzag or drop shape changers, with the S or drop type having the lowest pressure drop.

For the preliminary analysis only mechanical pressure-induced loading was considered, in this case a reference temperature of 550 ° C was used, representing the average temperature from the operating conditions of the exchanger, for a case using helium and s-CO2. For this, the geometry of a single S fin supported on a plate was used. As in this type of exchanger, the process of joining the plates is photochemical, the edges of the channel geometry are smoothed, reducing the region of stress concentration. To consider this effect, the edge geometry was smoothed with a radius of 0.1 mm. For loading, the prescribed uniform pressure condition was applied along the surfaces with a value of 20 MPa for the lower surface and 7 MPa for the sides.

At the tip of the S-profile, the local plastic strain is expected to be higher, for this reason the mesh should be better refined and the non-linear plasticity model should be applied. Due to the non-linearity of the simulation caused by plasticity, the convergence and Newton-Raphson residuals were activated to monitor the iterative solution process. In the case without thermal loading, the maximum stress value found is in the order of 150 MPa, occurring at the ends of the S-shaped geometry.

When analyzing multiple S fins, it was observed that the stress at the tip of the channel increased from 110 to 150 MPa. This behavior has a direct influence on the boundary conditions for a single fin. In this case, the condition of fixed support was used for the lateral surfaces of the plate, since the condition of symmetry together with the plasticity model resulted in divergences in the simulation. Thus, the supports used had a direct influence on the stress field found at the tip of the channel. As for the geometry with multiple channels, it was observed that there is less variation in the stress field due to the support region being further away. Based on this, it was concluded that the model using a single channel and fixed support at the edges of the plate is not representative enough to analyze the stress field. Figure 14 shows the difference in the stress field for increasing the number of channels.

Figure 14 – Difference between smaller and larger model.

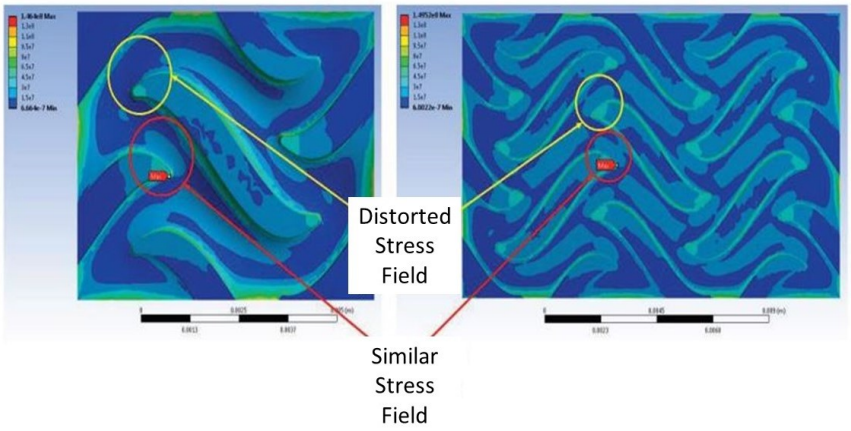

Source: Adapted from Zhang et al (2015)

Patil and Anand (2017) numerically analyzed the fatigue failure of shell and tube heat exchangers (STHE) using the ANSYS software. The cases were analyzed with separated thermal and pressure loading and later superimposed, where the mechanical loading was used in a prescribed way, while the thermal one resolved by finite differences only for the conduction heat exchange in the solid while the hydrodynamic loading was not solved.

To obtain the cyclic loading based on the standard (ASME Sec. VIII, Div. 2 Part. 5), two loading conditions were modeled, the first considering the temperature of 22 °C and 260 °C for the shell and tubes, respectively, named case 1. The second evaluating the temperature distribution with 160 ° C for the shell and 200 ° C for the tubes, named case 2. The pressure of the shell was kept constant at 6 MPa for both cases while that of the tube was varied between ambient pressure (0 MPa) and 2 MPa for cases 1 and 2, respectively. The loading curve per

number of cycles fluctuates between cases 1 and 2, representing the conditions for the start of operation of the exchanger and the steady state condition, as shown in Figure 15.

Figure 15 – Cyclic Load

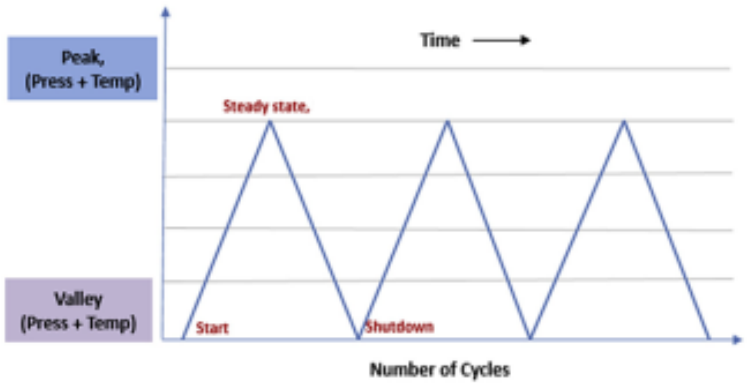

Source: Patil and Anand (2017)

The pressure load had higher peak values in the connection region between the tubes and the shell, and in general the thermal load had greater influence due to the oscillation of the pressure load and the high temperature gradient. The fatigue model indicated the maximum value of 341 cycles for the tubes and 1727 cycles for the shell, and in this stage fatigue life correction factors were disregarded or simplified, including for the welding regions. Figure 16 illustrates the difference between the effective and the thermal stress field across the exchanger.

Figure 16 – STHE: (a) Effective equivalent stress. (b) Thermal Stress.

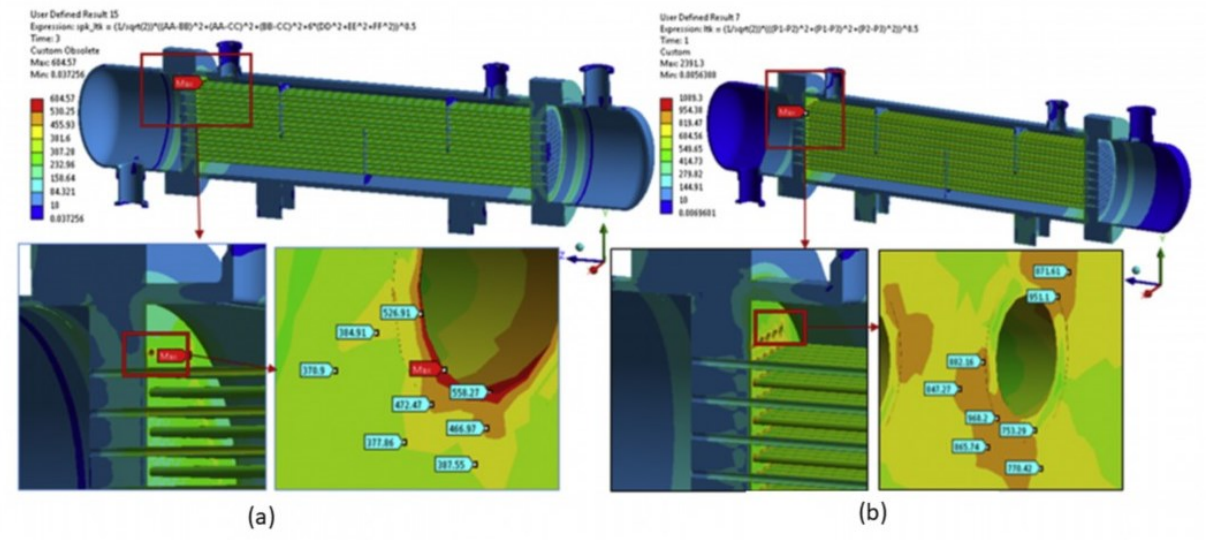

Source: Patil and Anand (2017)

Hou and Tang (2019) analyzed PCHE type heat exchangers applied to rocket engines. The exchanger uses helium and hydrogen as working fluids and has a square cross section with straight channels. In this type of exchanger, the number of channels is generally greater than 10^6 and the flow is laminar. For the study, a heat exchanger made of 316 stainless steel was used. To obtain the thermo-hydrodynamic behavior, simulations using the ANSYS Fluent program were performed for a geometric unit composed of a cold channel and a hot channel. For the channel containing hydrogen, the inlet temperature was maintained at 35 K and the outlet pressure was maintained at 20 MPa, for helium flow the inlet temperature was maintained at 700K and the outlet pressure at 60 MPa. The mass flow rate of hydrogen was varied between $5x10^{-8}$ to $2.5x10^{-7}$ kg/s while for helium between $1.4x10^{-7}$ and $9x10^{-7}$ kg/s, the Reynolds number ranging from 100 to 500, considering a laminar flow. Symmetry and periodicity conditions were applied to represent the effect of the exchanger on the unit (Figure 17). The results of the fluid-dynamic flow were validated with Nusselt data by Reynolds found in the literature (KIM; NO; LEE; JEON, 2009)

Figure 17 – PCHE model. (a) Unit cell dimensions and boundary conditions. (b) Scheme of the structure of the channels in a PCHE.

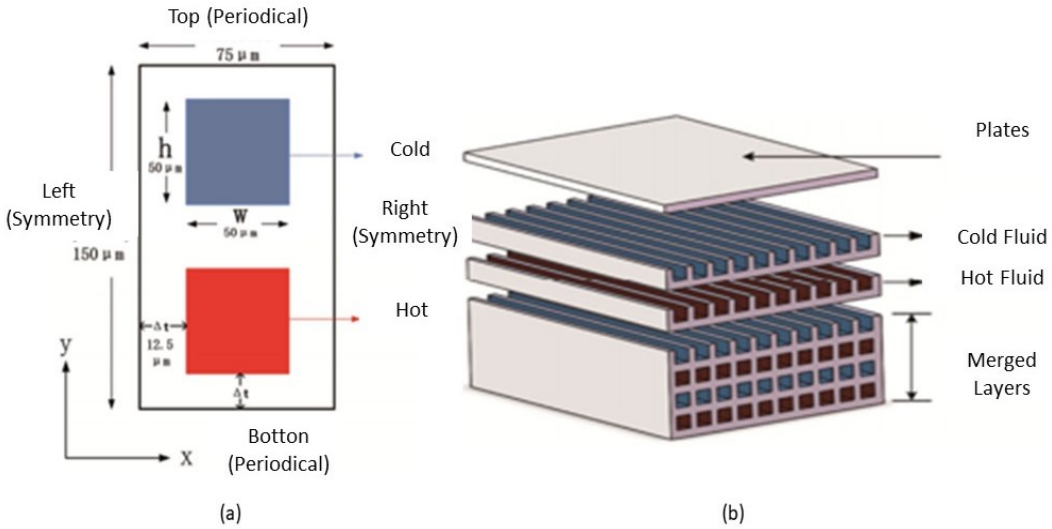

Source: Adapted from Hou and Tang (2019)

For the structural model, the geometry used consists of a PCHE unit containing 20 channels in 4 rows by 5 columns, where the edges of the channels were considered rounded with a radius of 1 µm. Only a piece of the channel is analyzed, 0.5 micrometers thick. The

region chosen is the hot fluid inlet because it presents the region with the highest temperature in the exchanger. Similar to the behavior found by Lee and Lee (2014), the temperature gradient tends to cause stress concentrations between the cold and hot channel, while the mechanical loading causes stress concentration at the vertices of the square, mainly for the cold channels. The stress found for the largest portion of the exchanger volume did not exceed 120 MPa, while for the region of concentration of stress of the channel the value 577 MPa was observed. When analyzing the stress field along the first row of channels, it can be seen that the stress distribution in the lower right corner is the same as in the upper left corner. The thermal stress at the corners of the channel is 2/5 of the value found for mechanical loading. In order to verify the influence of the channel geometry, the aspect ratio of the channel (w / h) was varied, where w is the width and h is the height. Thus, it was possible to observe that for higher values of w/h the average stress along the lower side of the channel decreased while the right side suffered a slight increase, stabilizing between 2 and 4. The percentage of plastic strain in the channel walls was also analyzed as a function of the aspect ratio, having a reduction from 20 to 7% for values of aspect ratio between 0.25 and 1, subsequently suffering an increase of 7 to 20% for values of aspect ratio from 1 to 4. The aspect ratio of 2 proved to be the ideal value in the relationship of mechanical and hydrodynamic behavior.

Li et al (2019) evaluated the structural performance of 3 pairs of titanium alloy PSHE type heat exchanger plates (TA1 and TA2) using the ANSYS program. In the model, constant properties were assumed with the temperature for TA1 titanium alloy, in addition to the fatigue life curve for up to 10^6 cycles, considering cyclic loading varying between 50 and 100% of the maximum load found in the static simulations. The titanium alloy was assumed to be ductile, allowing the use of the Gerber failure criterion for medium stress. In the study, uniform pressure loading of 2 MPa was used inside the channels of the plate.

For static loading, the maximum stress was found close to the weld region at the edge of the plate, reaching values of 226.89 MPa, as shown in Figure 18. Fatigue tests indicated that the plate has a minimum life of 3000 cycles and that the weld region is the most likely to fail.

Figure 18 – PSHE stress field.

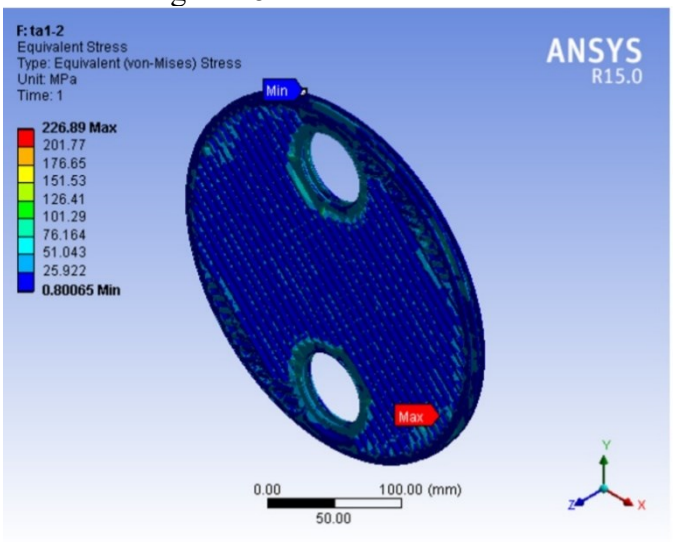

Source: Li et al (2019)

Pelliccione et al (2019) evaluated the failure of PHE type heat exchangers for applications in the oil and gas industry using the ANSYS software. The exchanger used in the work was removed from real operating conditions after the failure, using seawater and clean water as working fluids. The seawater channel has an inlet temperature of 29°C and a pressure ranging between 0.6 and 0.8 MPa, while the channel with clean water has an inlet temperature of 32°C and a pressure ranging between 0.3 and 0.4 MPa. In this condition, the exchanger made with 0.6 mm plates of titanium alloy ASTM B265 Grade 1 failed in 126000 hours of operation.

Plate samples were cut in regions that showed macro cracks in visual inspections, cracks that appeared mainly in the plate sealing region. In the crack region, the brittle phase of titanium hydride was identified, which favors the propagation of cracks in titanium alloys.

Subsequently, the exchanger plate was scanned using a 3D laser with 0.5 mm resolution to obtain geometry (Figure 19 (a)). In the model, the surface in contact with sea water has a prescribed pressure load of 0.3 MPa. The internal surface in contact with fresh water, it has a prescribed pressure of 0.8 MPa. The gasket region was prescribed with a sealing pressure of 2 MPa. Residual stresses from the forming process for the manufacture of the plate were not considered. At the vertical edges of the plate, the condition of fixed support for the x and z directions, while for the vertical edges, at y and z. The numerical model showed a region with greater stress in the same region where cracks were identified (Figure 19 (b)).

Figure 19 – PHE Samples. (a) Scanned regions. (b) Stress field for the tested section.

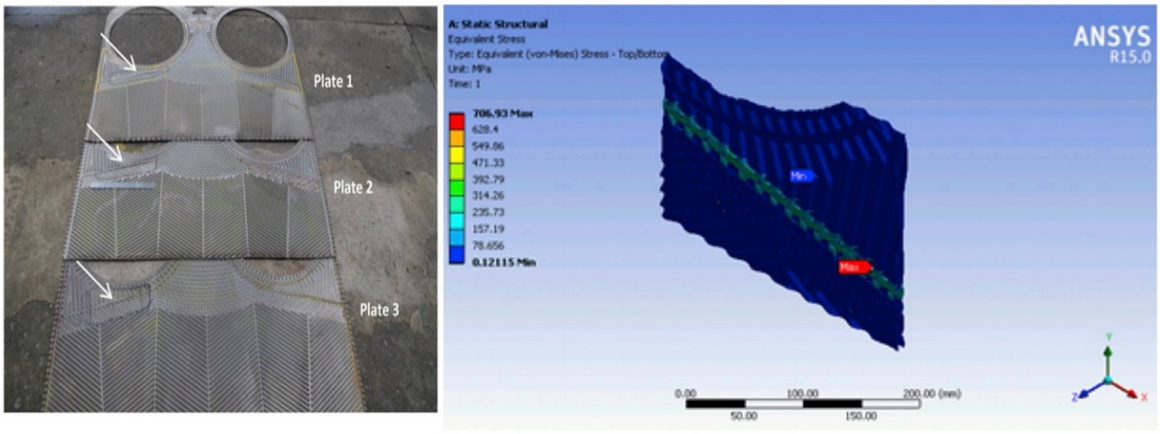

(a) (b)

Source: Pelliccione et al (2019)

Donati (2019) performed analyzes of the fluid-structure interaction of pairs of PSHE type heat exchanger plates for a Chevron angle of 45 °. The thermal and pressure loads were obtained using the same methodology proposed by Taschеck (2019), using the ANSYS CFX software.

The pressure loading was more intense close to the region of the entrance edge of the plate, having its effect reduced due to the loss of pressure along the channels. As for the temperature loading, as the temperature variation between the initial state of the fluid and the solid was very small, the temperature gradient for the case studied was practically zero.

The pressure and temperature fields were introduced in the ANSYS Static Structural program as a loading. Pressure and temperature loads were evaluated separately to assess which has the greatest effect on the geometry of the plate. The mechanical properties used in the study, taking into account the temperature variation during the operation and mechanical property variations due to welding, were obtained from Song and Hong (2013).

In the model, two plates were used, connected by a circular ring with a square section 1 mm thick to represent the weld. The contact used between the plates and the solder was the fixed type (“Bounded”). For contact between the plates, the frictionless contact condition was used. The condition of free circular displacement was imposed on the weld geometry only in the radial direction. The ports were modeled with free circular displacement only in the axial direction. The pressure loading used was obtained for a water flow condition of 0.344 Kg/s at the inlet with an initial fluid temperature of 90 °C and the solid varied between 30, 62.5 and

75°C , named cases 1, 2 and 3, respectively. The case named 4 was the only one with coupled loading, replicating the conditions of case 2. The external surfaces of the plate were modeled as adiabatic. It is important to note that higher temperature gradients have an influence on the pressure field obtained through hydrodynamic simulations, therefore, affecting the stress state of mechanical loading.

For isolated pressure loading, the plates do not have deformation restrictions on the corrugations, showing displacement in a preferred direction following the plate corrugations, as shown in Figure 20(a). When evaluating the directional displacement following the preferred direction of the channels, one can observe the greater intensity of displacements near the edge of the plate, at the end of the channels, as shown in Figure 20(b).

The increase in the temperature gradient between the solid and the fluid caused an increase in the stress intensity found on the corrugations when analyzing the pressure loading, with the weld regions showing higher stress values, as shown in Figure 20(c). The maximum stress value found is located close to the inlet port region due to the pressure drop.

Figure 20 – Behavior for pressure loading. (a) Total displacement field. (b) Directional displacement. (c) Von Mises stress field.

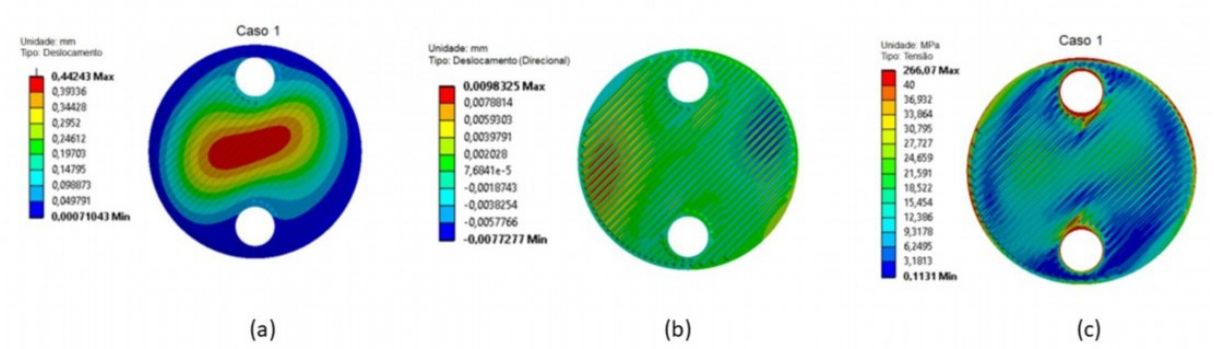

Source: Donati (2019)

Thermal loading also showed a preferential direction, having greater influence the greater the thermal gradient found (Figure 21 (a)). In this case, the preferred direction found is orthogonal to the direction of the channels. The stress field also showed greater magnitude due to the increase in the temperature gradient, but the concentration of stress occurred between the entrance and exit edges of the plates, since this is the temperature gradient direction (Figure 21(b)). As the temperature gradient is very low, the stresses found for thermal loading are 200 times less intense than the stresses for pressure loading:

Figure 21 – Thermal loading Behavior. (a) Total displacement field. (b) Von Mises stress field.

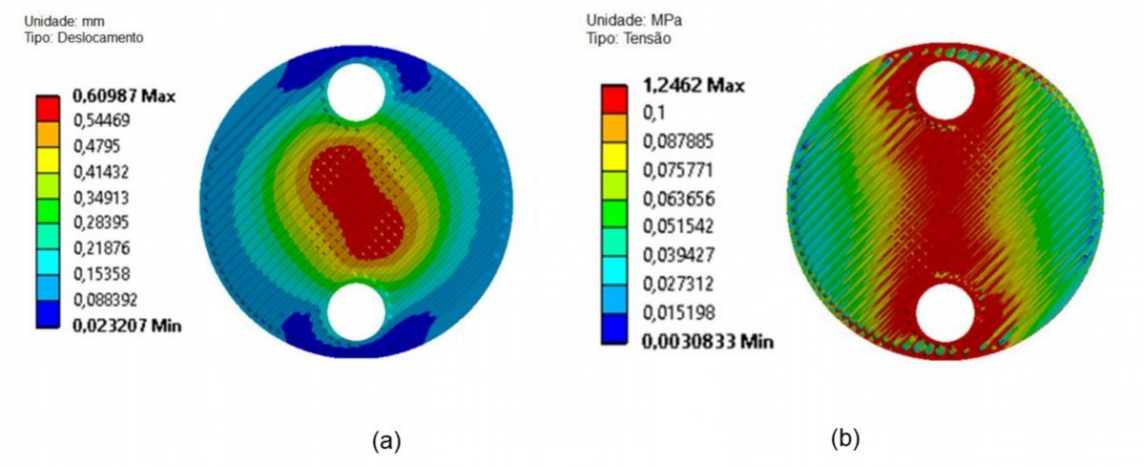

Source: Donati (2019)

Finally, when evaluating the coupled loading, it can be seen that the total displacement field (Figure 22(a)) and von Mises stress field (Figure 22(b)) have a strong influence of the preferred directions of the thermal and pressure loads overlapping. At the crossing points of the loads, the stress becomes higher, causing the channels to flatten as a result of the contact points. In addition, the stress found in the coupled load is an order of magnitude greater than that found in the pressure load. All results were considered qualitative since there was no data to validate experimentally.

Figure 22 – Coupled loading behavior. (a) Von Mises displacement field. (b) Von Mises Stress Field.

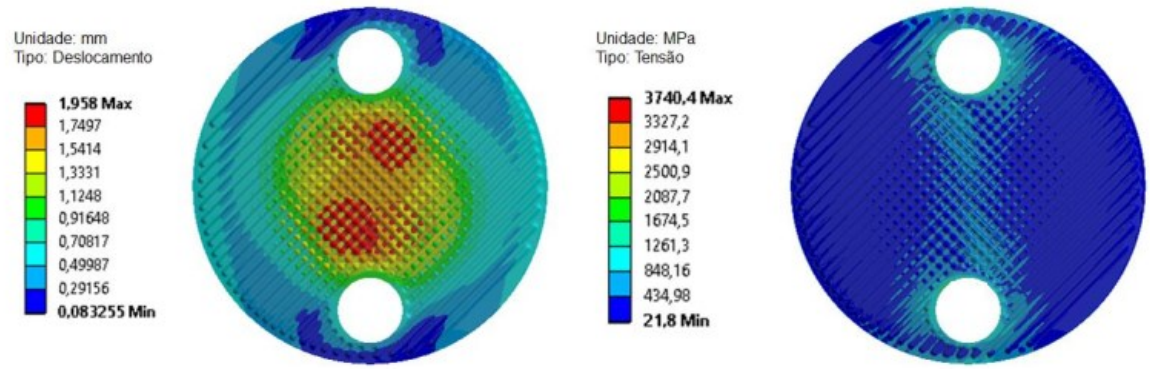

Source: Donati (2019)

Martins (2020) experimentally estimated the fatigue life curves for a PSHE for pressure values between 1 and 1.4 MPa, in this case considering repeated loading. The fatigue

analysis was based on the ASME standard to determine the life of the exchanger as a function of measurements made with triaxial extensometers and to determine fatigue life reduction factors for weld regions. This geometry region presented a greater number of failures for this type of exchanger. Initially, as a way of validating and calibrating the bench, pressure vessels of the R22 type were tested because they are simple geometries and an analytical approach well developed in the literature, in addition to having multiple welds throughout their construction. These tests showed deviations of 8% for the cylindrical region of the pressure vessel and about 30% for the torospheric region, with a failure in the central weld region.

Subsequently, a single pair of pressurized plates was tested to obtain fatigue life curves under different conditions, noting that the exchanger also failed in the welded region. It was also found that the range of values for the fatigue life reduction factor found in the standard (ranging from 1 to 4) is smaller than that needed to calculate the element's fatigue life adapting the standard methodology from a pressure vessel to a heat exchanger. The ideal value found for the corrugated plate is 6.2.

Figure 23 shows the stresses found for the pair of plates. It is important to note that due to the geometric conditions of the plate, it was not possible to add strain gauges along the channels. The white dash line is added to explain geometry characteristics, in which regions 1 and 2 presents similarities.

Figure 23 - Effects of PSHE plate geometry and test pressure equal to 1.4 MPa on equivalent stress values at the ends of the plate pair. Measurements at points 7 to 12 (left, a) and 1. to 6 (right, b). The plate on the right (b) contains the pressure port on the lower port.

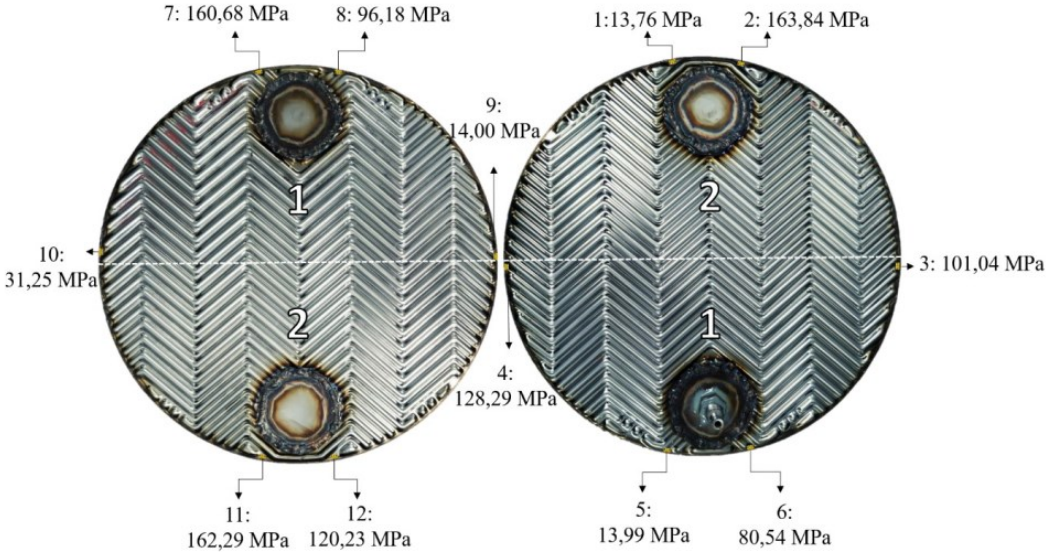

Source: Martins (2020)

Analysis were also carried out to check the influence of different tightening or spacing between the pairs of plates in order to identify variations in the equipment's life. For cases where the tightness is high, the service life has increased considerably, with behavior inversely proportional to the increase in spacing. This parameter is important because during the operation of the exchanger, the higher the pressure values of the working fluids, the greater the chance of separation between the plates and, consequently, the shorter the life of the equipment.

Hyun-Seok, Jong-Rae and Seung-Hun (2020) evaluated the structural behavior of a straight channel PSHE made from Titanium. Numerical models in elastic and elastoplastic regimes were developed, evaluating the results using the ASME standard (ASME Boiler and Pressure Vessel Code, Section VIII Division 2).

The models of one and two pairs of plates were made considering only a quarter of the plate to reduce computational cost, evaluating the use of solid and surface bodies, as shown in Figure 24. The use of surface bodies in detriment of solid bodies allows the reduction of computational cost, since in this configuration it is not necessary to use mesh elements along the thickness of the body. This approach is only valid for plates with small thickness and considers only tangential stresses to the plate surface (membrane stress). None of the models had a distinct region for the weld.

The nodes in the region of symmetry were fixed in the normal direction to the cross-section area, the contact between the plates was modeled as two independent bodies leaning against each other and on the external plates the displacement in the vertical direction was limited. The prescribed pressure loading of 11.8 MPa was applied to the outer surfaces of the pack.

Figure 24 – FE modeling schemes for a (a) two-layer solid. (b) two-layer shell, and (c) four-layer shell.

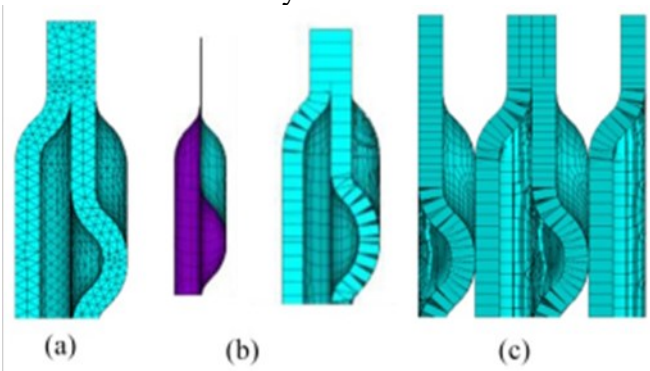

Source: Hyun-Seok, Jong-Rae and Seung-Hun (2020)

The results show that the stress field was similar for all cases, with peaks in the contact region. The values in the contact region for the elastic model were higher compared to the elastoplastic model, due to the plasticization effect. Peaks of stress were also found along the weld region indicating a possible failure region, as shown in Figure 25. The model using surface elements proved to be valid, suffering less effect from boundary conditions. The use of plasticity models proved to be more appropriate due to the appearance of adverse stress peaks in the contact region during elastic analysis.

Figure 25 – Stress field in a PSHE.

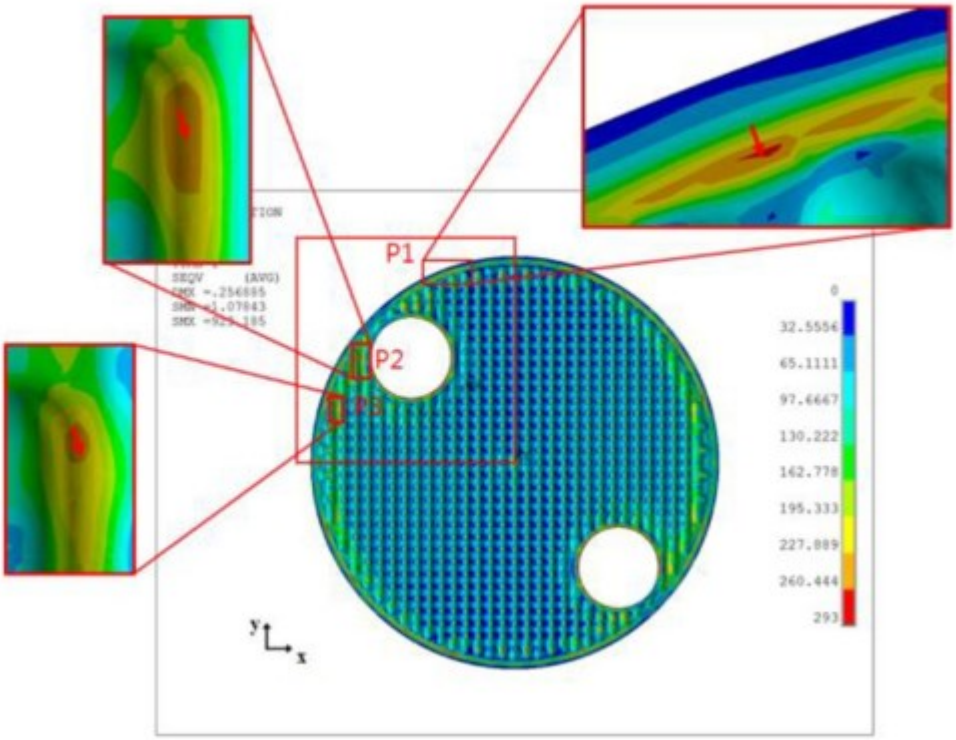

Source: Hyun-Seok, Jong-Rae and Seung-Hun (2020)

Table 3 presents the main information of the references. Of all the articles presented, it is important to mention that few used a distinct weld geometry to assess the failure of a component, and that this region is directly linked to the failure of the heat exchanger. Even though this is not the focus of this work, references were found that evaluate the plasticity effects in different regions of the heat exchanger. This material behavior, when considered, tends to reduce peak stress values in the plasticized region. This behavior occurs because the numerical model maintains its dependence on the Young's modulus, even after exceeding the

Yield limit. Finally, although there are studies that evaluate the fatigue behavior of the heat exchanger, they are not very detailed and lack experimental validation. This is the greatest contribution that this work seeks to achieve.

Table 3 – Article's resume.

Author	Year	Type	Resume	Study focus	Results
Song	2011	Numerical	It solved the heat conduction in the exchanger and the stress analysis through finite elements using the ABAQUS program. The hydrodynamics of the flow was not resolved, the pressure loading being prescribed in the solid.	PCHE with straight channels at 950 °C	Indicates that the stress due to thermal loading at high temperatures is more significant than pressure
Song Hong e Park	2012	Numerical	It evaluated the effect of the welds used in the manufacture of the exchanger to reduce the life of the component by evaluating the average properties along the weld as a function of the modulus of elasticity and ultimate stress of the base material. The thermal loading was obtained by conducting heat in a numerical way using the ABAQUS program.	PCHE with straight channels at 850 °C	The maximum stress is found on the plates that seal the exchanger, close to the weld region. The maximum stress value tends to decrease when considering the chamfers applied over the region.
Song e Hong	2013	Numerical and Experimental	It solved the heat conduction in the exchanger and the stress analysis through finite elements using the ABAQUS program. The hydrodynamics of the flow was not resolved, the pressure loading being prescribed in the solid. He accounted for the effect of the variation of properties with temperature and welding.	PCHE with straight channels at 700 °C	Identified that the modification by the effect of the weld leads to the concentration of stress in this region.

Author	Year	Type	Resume	Study focus	Results
Lee e Lee	2014	Numerical	Solved the heat conduction (finite volumes) in the exchanger and the stress analysis (finite elements) by analyzing the influence of plasticity models on structural behavior using the ANSYS program. Modeling in representative cells of the exchanger in 2x1, 4x4 and 8x8 channel configurations was also analyzed.	PCHE (Semicircular channels)	For the temperature range analyzed, the stress due to mechanical load was more significant. Furthermore, the study indicates that for this type of exchanger the minimum representative model must be 4x4 channels.
Nascimento	2013	Numerical and Analytical	Developed and applied a 1D (algebraic) and 2D (numeric) model to estimate points of failure in the operation of the heat exchanger. Included the gasket effect in the 2D model. Evaluated the stress field along the gasket and plate channel through numerical simulations of part of a PHE heat exchanger plate, taking into account the use of elastic supports to represent the gasket and the contact between multiple plates.	GPHE	He identified that the plates of the exchanger can be represented by a medium displacement and that the contact points between plates have zero displacement. With the three-dimensional model, it was verified that considering the sealing pressure specified by standard, there is no failure of the exchanger due to leakage. For the corrugation region, the maximum stress is found at the points of contact between the plates, with a value of up to 100 MPa.

Author	Year	Type	Resume	Study focus	Results
Zhang et al	2015	Numerical	It solved the mechanical structural analysis with prescribed pressure on the model's faces (without thermal stress) for a representative exchanger's geometry and for a complete geometry of the plate. Employed nonlinear plasticity model present in ANSYS Mechanical	S-shaped fin PCHE	Concluded that the smaller model behaves differently from the complete model of the plate (stress difference at the end of the S channel from 110 to 150 MPa) indicates that proximity to the boundary conditions is important.
Zhang et al	2015	Numerical	Numerically evaluated the thermal hydrodynamic performance through numerical simulations using the ANSYS software, which were later validated with the aid of an experimental bench. Subsequently, the pressure and temperature fields were imported for the structural analysis of the component using a fluid structural approach.	PFHE	Compared how different geometry configurations can influence the exchanger's performance and its structural integrity, correlating the Reynolds number with the maximum stress.
Pantil e Anand	2017	Numerical	He solved the structural analysis evaluating the mechanical and thermal load, separately and together using ANSYS. The thermal analysis was made based only on the resolution of the heat exchange by conduction in the solid. It did not consider correction or differentiation factors for the weld regions.	STHE	For the analyzed cases, the thermal stress was more significant than the mechanical stress. The fatigue model indicated shorter fatigue life for the tubes. Alternating loading with non-zero mean was employed.

Author	Year	Type	Resume	Study focus	Results
Hou e Tang	2019	Numerical e Experimental	It evaluated the performance exchanger and experimentally obtained Nu and Re curves together with the pressure and temperature fields. Subsequently, a structural fluid analysis was performed using ANSYS mechanical, where the pressure and temperature range was used as loading for different configurations of the exchanger. The thermo-hydrodynamic behavior of the exchanger was validated by Kim, No, Lee and Jeon (2009).	PCHE of square cross section and straight channels	Evaluated plasticity effects along the changer corners as a function of the aspect ratio of the channel, showing that for channels with square cross section, the aspect ratio 2 between the height and width of the channel is ideal to guarantee the best structural integrity without compromise performance.
Li et al	2019	Numerical and Analytical	Analyzes the heat exchange in a titanium PSHE and solves numerically the static structural problem (ANSYS Mechanical) for alternating cycle fatigue analysis with average. The structural analysis is performed only for 3 pairs of plates. The weld was not considered as a modified material.	PSHE	With the use of a uniform load of 2 MPa inside the central pair of plates, the maximum equivalent stress found was around the weld of the plate edge, indicating that this would be the most likely place of failure due to mechanical fatigue.
Pelliccione	2019	Numerical e Experimental	Evaluated the failure of a PHE heat exchanger through metallographic analysis and a finite element model using the ANSYS program.	GPHE	He found cracks in the seal area of the plate with the gaskets, probably due to the reverse buckling load. The finite element model used the average working pressure of the exchanger and a sealing pressure equivalent to 2 MPa (according to the ASME standard for pressure vessels Sec. VIII, Div. 1.

Author	Year	Type	Resume	Study focus	Results
Donati	2019	Numerical	Evaluated the fluid structural behavior of PSHE type plate exchanger pairs on the isolated and coupled influence of pressure and temperature loads.	PSHE	The loadings showed the preferred direction of displacement on the corrugated plate, parallel to the corrugations for pressure loading and orthogonal for thermal. The weld region showed the highest stress concentration for the pressure loading and the region between the inlet and outlet ducts for the thermal. Coupled loading showed flattening in the channels, with stresses an order of magnitude higher than pressure loading
Martins	2020	Experimental	Experimentally obtained the fatigue life curve for plate heat exchangers. He validated the experiment using R22 pressure vessels because they are simple geometries and easy to analyze. Component life was estimated using strain measurements using triaxial strain gauges and the ASME standard.	PSHE	It determined that for the plate pairs the fatigue life reduction factor due to the weld is 6.2, although the standard determines values between 1 and 4. The welds along the perimeter of the plates had the highest incidence of flaws

Author	Year	Type	Resume	Study focus	Results
Hyun-Seok, Jong-Rae and Seung-Hun	2020	Numerical	Evaluated the stress field in a PSHE with straight channels made out of titanium. Analyzed different geometric configurations and the elastic-plastic behavior of the material	PSHE	Concluded that the use of shell elements together with the elastoplastic model better represent the structural behavior of a PSHE with low computational cost. The weld's region is the most likely to fail during the operation of the exchanger.

Source: Author (2021)

3 FINITE ELEMENT METHOD

The Finite Element Method (FEM) applied to structural problems is a numerical method for discretizing differencial equations that when applied to structural problems, can be used to obtain the displacement, strain and stress fields in complex geometries. The explanation, hypotheses and deduction of the equations that represent phenomenology can be found in more detail in different literature. Among them, Cook (1995) will be used here as a basis. The great advantage of this method is its versatility, since the geometry can be complex, having supports and arbitrary loads, which results in greater flexibility when compared to analytical methods. In addition it allows the achievement of the complete stress state of a given piece at a time, something that can only be achieved in experimental methods with multiple extensometers. The same can be said of loads induced by thermal loads, regardless of the complexity of the temperature profile present in the part.

In a simplified way, FEM consists of sectioning the geometry of the part to be studied in smaller elements, where the behavior of each element is analyzed. The elements are connected by nodes, similar to the functioning of a pin between two links, with each element having a node for each end, totaling 2 nodes per element. This arrangement is named mesh. With this modeling, a set of algebraic equations is obtained from partial differential equations that allow relating the displacement of the nodes as a function of applied forces, and the equilibrium equations describe the displacement of each node, being proportional to the number of nodes in the mesh. From the nodal displacements, the strain and strain field can be obtained. Figure 26 illustrates a generic case, where the lines represent the elements, which are connected by the nodes (points), where u and v indicate displacement in the x and u axis respectively and P is the force applied. In this case, it can be noted that the problem is two-dimensional.

Figure 26 – Nodal displacement

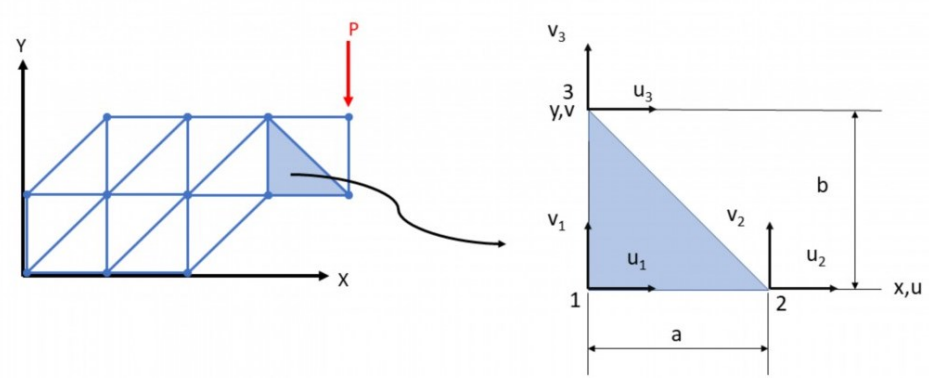

Source: Author (2021)

The main default simplifying hypotheses for the FEM are:

- 4 plates simplified model, following the same approach used by Martins (2020) and Nascimento (2013);
- Strain in the material occurs in the elastic regime, therefore plastic strain are disregarded;
- The material is linear isotropic;
- Strain and displacements must be small.

In this work theses three hypotheses are considered. It is important to highlight here that there models that can consider plastic behavior of the material and anisotropic materials but they are not applied in this work.

3.1 NON LINEARITIES IN FEM

In linear analysis, it is assumed that the displacements and rotations are small, that the stress is directly proportional to the strain and that the load maintains its original direction as the structure deforms. For cases in which the material starts to plastically deform or without a linear relationship between the stress and strain curve, or in which variations in the stiffness of the structure as a result of the deformation, the displacements and rotations become high, in this case the equations of balance should be written for the deformed configuration.

Cases in which non-linearity effects occur are much more complicated because the equations that describe the problem depend on conditions not fully understood before the solution. In this case, the solution must go through iterative processes until a certain convergence criterion is reached. Plastic strain or large displacements are not met by the model used in this work and therefore the results that exceed the material Yield's limit or that present high displacement should be treated as qualitative.

3.2 FATIGUE

Fatigue is the material weakening process caused by a cyclic loading resulting in structural damage and growth of cracks. Unlike yielding process, fatigue fail is sudden, failing in a lower stress level than yield limit. The explanation, hypothesis and deduction of the

equations that represent the phenomenology can be found in more detail in different literature. Among them, Norton (2013) and Budynas et al. (2015) will be used here as a basis.

Other than yield, fatigue stress vs number of cycles curves are much harder to be obtained than stress vs strain curves. One way to estimate the material weakening as a function of the number of cycles is evaluating the maximum stress level, where the function is valid between 10^3 and 10^6 cycles (high cycle fatigue).

The fatigue resistance (S) curve for the material can be obtained as a function of the number of cycles (N) and by boundary condition's constants (a and b), as shown in below:

$$S(N) = aN^b \tag{1}$$

To obtain the constants a and b the same equation can be expressed as a log-log function:

$$logS(N) = \log(a) + blog(N) \tag{2}$$

Knowing that S(N) = S_m when N =N_1 = 10^3 and S(N) = S_e when N =N_2 = 10^6, the previous expression can be written as shown in bellow to find a and b:

$$b = \frac{1}{z}\log\left(\frac{S_m}{S_e}\right) \; where \; z = \log(N_1) - \log(N_2) \tag{3}$$

$$\log(a) = \log(S_m) - blog(N_1) = \log(S_m) - 3b \tag{4}$$

Its important to note that S_m and S_e are dependents of the Ultimate Tensile Stress (S_{ut}) of the material, where $S_m = 0.9S_{ut}$ and $Se = 0.5S_{ut}$, where C is a constant dependent of multiple factors, such as temperature, surface finish, reliability and manufacturing process.

In order to evaluate if the fatigue failing is occurring, it is important to know the behavior of the load, since the same conditions used by Martins (2020) will be used in this work. A repeated load can be described as wave form cyclic load ranging from zero to the maximum stress, with the alternated stress(σ_a) equal to the mean stress (σ_m), as shown in Figure 27.

Figure 27 – Repeated load

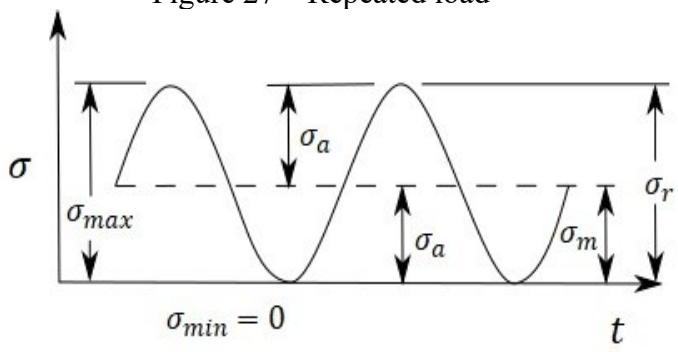

Source: Budynas et al. (2015)

The Gerber, Goodman and Soderbeg fatigue failure criteria are presented below, respectively:

$$\begin{aligned} &\frac{\sigma_a}{S_e} + \left(\frac{\sigma_m}{S_{ut}}\right)^2 = 1 \text{ (Gerber)} \\ &\frac{\sigma_a}{S_e} + \frac{\sigma_m}{S_{ut}} = 1 \text{ (Goodman)} \\ &\frac{\sigma_a}{S_e} + \frac{\sigma_m}{S_y} = 1 \text{ (Soderberg)} \end{aligned} \tag{5}$$

As seen in Martins (2020) and in Patil and Anand (2017), the effective equivalent stress range can be computed from alternating stress equation, using the equivalent stress tensor ($\Delta\sigma_{ij,k}$) for the starting (time ^{m} t) and ending (time ^{n} t) points of a cycle of a given global load (k), representing peak (m) and valley (n) conditions. The von Mises stress criteria can be used to determine the equivalent mechanical ($\Delta S_{p,k}$) and thermal ($\Delta S_{LT,k}$) stress ranges. The mechanical stress equations are shown below:

$$\Delta\sigma_{11} = (\sigma_{11} - \sigma_{11}^{LT})_m - (\sigma_{11} - \sigma_{11}^{LT})_n \tag{6}$$

$$\begin{aligned} &\left(\Delta S_{p,k} - \Delta S_{LT,k}\right) \\ &= \frac{1}{\sqrt{2}}[(\Delta\sigma_{11} - \Delta\sigma_{22})^2 + (\Delta\sigma_{11} - \Delta\sigma_{33})^2 + (\Delta\sigma_{22} - \Delta\sigma_{33})^2 \\ &+ 6(\sigma_{12}^2 + \sigma_{13}^2 + \sigma_{23}^2)^{0.5}] \end{aligned} \tag{7}$$

In which $\Delta S_{p,k}$ is the range of the primary plus secondary plus peak equivalent stress and $\Delta S_{LT,k}$ is the Local thermal equivalent stress. Similarly, for the thermal stress equations:

$$\Delta\sigma_1^{LT} = \sigma_1^{m\,LT} - \sigma_1^{n\,LT} \tag{8}$$

$$\Delta S_{LT,k} = \frac{1}{\sqrt{2}}[(\Delta\sigma_1^{LT} - \Delta\sigma_2^{LT})^2 + (\Delta\sigma_1^{LT} - \Delta\sigma_3^{LT})^2 + (\Delta\sigma_2^{LT} - \Delta\sigma_3^{LT})^2 + 6]^{0.5} \tag{9}$$

The effective alternating equivalent stress amplitude ($S_{alt,k}$) can be calculated:

$$S_{alt,k} = \frac{K_f K_{e,k}\left(\Delta S_{p,k} - \Delta S_{LT,k}\right) + K_{v,k}\Delta S_{LT,k}}{2} \tag{10}$$

In which K_f is the fatigue strength reduction factor, $K_{e,k}$ is the fatigue penalty factor and $K_{v,k}$ is the Poisson correction factor. Table 4 and Table 5 present the set of necessary settings to define the fatigue strength reduction factor (K_f).

It is important to note that the ANSYS Static Structural program only allows the use of the fatigue strength factor to take into account real environmental problems that can cause fatigue life reduction, considering the effect of $K_{e,k}$ and $K_{v,k}$ on a single factor mixed with K_f. This factor can be used to consider surface finish, discontinuity in the material properties along the weld zone and others. Differently from the theory presented above, ANSYS K_f factor is inversed, with a range of 0.01 and 1.

Table 4 - Weld Condition and Quality Level.

Weld Condition	**Surface Condition**	**Quality Level (See** Table 5**)**						
		1	**2**	**3**	**4**	**5**	**6**	**7**
Full Penetration	Machined	1	1.5	1.5	2.0	2.5	3.0	4.0
	Without treatment	1.2	1.6	1.7	2.0	2.5	3.0	4.0
	Final machined surface	NA	1.5	1.5	2.0	2.5	3.0	4.0
Parcial Penetration	Untreated final Surface	NA	1.6	1.7	2.0	2.5	3.0	4.0
	Root	NA	NA	NA	NA	NA	NA	4.0
Fillet Weld	Machined weld margin	NA	NA	1.5	2.0	2.5	3.0	4.0
	Untreated weld margin	NA	NA	1.7	2.0	2.5	3.0	4.0
	Root	NA	NA	NA	NA	NA	NA	4.0

Na - Not Available.

Source: Adapted from ASME (2015)

Table 5 - Welding surface: fatigue strength reduction factor (K_f).

K_f	Quality Level	Definition
1.0	1	Machined or rectified weld that receives complete volumetric examination and a surface that receives MT/PT and VT exams.
1.2	1	Untreated weld that receives complete volumetric examination and a surface that receives MT/PT and VT exams.
1.5	2	Machined or rectified weld that receives partial volumetric examination and a surface that receives MT/PT and VT exams.
1.6	2	Machined or rectified weld that receives partial volumetric examination and a surface that receives MT/PT and VT exams.
1.5	3	Machined or rectified weld surface that receives MT/PT examination and VT (visual) exam, but the weld is not inspected by exam volumetric
1.7	3	Machined or rectified weld surface that receives MT/PT examination and VT (visual) exam, but the weld is not inspected by exam volumetric
2.0	4	The weld received a partial or total volumetric examination, and the surface received a VT exam and no MT/PT exam.
2.5	5	VT examination of surface only; no volumetric exam or exam MT / PT.
3.0	6	Volumetric exam only
4.0	7	Weld type not defined and/or not receiving any exams.

(1) Volumetric analysis is performed via ultrasonic (UT) or radiation (RT) testing, done in accordance with part 7 of the code.

(2) MT/PT exams: magnetic particle or liquid penetrant, done according to part 7 of the code.

(3) VT Examination: Visual examination performed in accordance with part 7 of the code.

Source: Adapted from ASME (2015)

4 HEAT EXCHANGERS ANALYSIS METHODOLOGY

The present work was carried out with the aid of commercial programs to assess the physical phenomena that occur during the operation of the exchanger.

The computational tools used were: Solidworks and ANSYS Design Modeler 18 for the design of geometries, ANSYS Meshing for obtaining the mesh and ANSYS Static Structural for the resolution of stresses and displacements taking into account the effects of non-linearity.

At this stage, it is important to highlight the work developed by Martins (2020). As the geometry analyzed for the PSHE with zigzag channels is the same studied in this work, the same boundary conditions were replicated, as well as the geometry and supports configuration to evaluate the equipment structural behavior. The description of the geometries, meshes and boundary conditions used will be shown below.

4.1 PSHE PLATE'S GEOMETRY AND MATERIAL PROPERTIES

Figure 28 shows the PSHE plate geometry studied in the present work, which is produced from 316L stainless steel. The plate has zigzag channels with an inclination of 36,87°. To represent the welds, a rim-shaped geometry was modeled with a 1 mm thick square cross-section, allowing the coupling between different plates.

Figure 28 – PSHE plate dimensions and configuration.

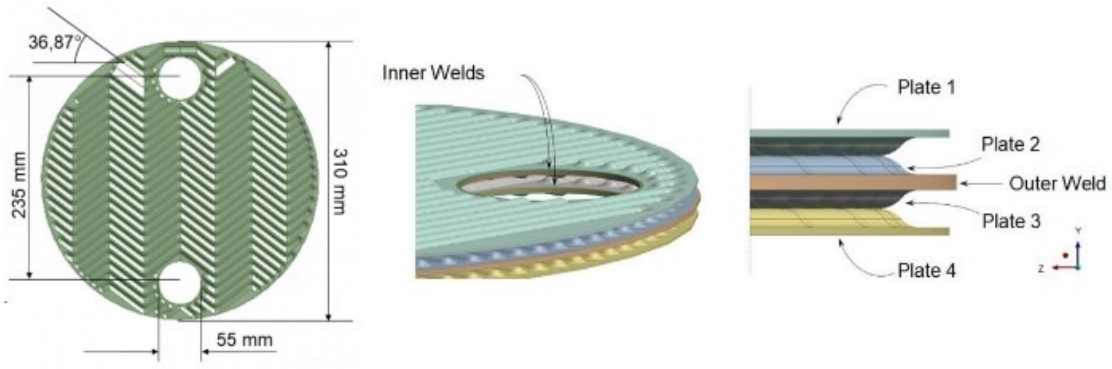

Source: Author (2021)

Due to the presence of welds, variations in the microstructure of the material are expected to occur. For this reason, the work of Song and Hong (2013) will be used as a basis to take this effect into consideration, and the values found are normalized based on the properties

of the base material. It will also be used the base material properties to see the difference in the weld behavior in static and fatigue loading. Cases with different material and equal to the base material will be called complex and simple weld models, respectively.

As seen by Nascimento (2013), the plate is expected to be orthotropic, having multiples elasticity modulus depending on the region and direction of the corrugation. However, in this work, the plate will be simplified as isotropic.

Table 6 shows the material properties of 316L Stainless Steel used in the plate's base material and in the welds. The properties for the base material are the same used by Martins (2020). The same relation used by Song and Hong (2013) to estimate the weld material mean properties were used to estimate the weld properties for this study, based on the material properties used by Martins (2020). Figure 29 shows the base material and weld alternating stress curve up to 99000 cycles.

Table 6 – 316L material properties.

Properties	**316L – Base Material**	**316L – Weld**
Density	8 g/cm³	8 g/cm³
Young's Modulus	195 GPa	218 GPa
Poisson's Ratio	0.31	0.31
Tensile Yield Strength	170 MPa	190 MPa
Tensile Ultimate Strength	485 MPa	545 MPa

Source: Author (2021)

Figure 29 – Alternating stress curves.

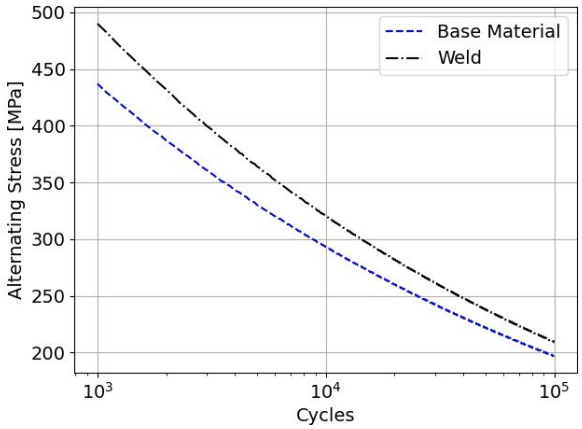

Source: Author (2021)

4.2 BOUNDARY CONDITIONS

The contacts are defined through the surfaces in contact between two or more bodies, and there may be restrictions on sliding between the bodies or not and restrictions on the separation between the surfaces of the bodies or not.

The *rough contact* allows the separation between contact surfaces, however sliding is not allowed, having an infinite friction coefficient ($\mu=\infty$). This condition was studied by Nascimento (2013) and proved to be adequate to represent the contact between the plates of the heat exchanger.

Another alternative to represent the contact between the plates is the *frictionless contact* allowing the sliding between the surfaces with zero friction coefficient ($\mu=0$) and the separation of the contact surfaces. This condition was also studied by Nascimento (2013) and there was no significant difference in the results obtained. The same condition was used in the work of Donati (2019).

The *bounded contact* is used to represent conditions where the bodies do not have any separation between the surfaces or sliding, being indicated here to represent the condition between the welds and the plates. This condition was also used by Pelliccione et al (2019) to represent the contact between the plates, assuming that the separation and sliding do not occur during the operation of the exchanger, a condition that was observed by Nascimento (2013).

For supports the condition of *fixed support*, *elastic support* and *displacement* can be used. The fixed support condition restricts all directional and rotational degrees of freedom, prescribeing the displacements as zero on these surfaces. The *elastic support* allows the faces to move or deform according to the behavior of a linear spring, defined from a foundation stiffness (“Foundation Stiffness”). Foundation stiffness is a volumetric stiffness defined as the pressure required to produce a normal unitary deflection of the foundation. The *displacement* condition specifies the displacement of a body from its original location. The displacement in a given direction can be defined as constant, null or free displacement. Nascimento (2013) used this condition to consider the gasket effect on the plate of a gasketed plate heat exchanger.

The prescribed pressure loading is a condition of uniform loading on the surfaces of a given geometry. This condition is normally applied to the surface and can be applied to flat or curved surfaces.

4.2.1 PSHEs Pressure Loading Boundary Conditions

Figure 30 shows the geometry configuration used for the PSHE model and the welds (represented in green) present in the model, with the boundary conditions applied shown in Table 7.

The fixed support condition was applied to all surfaces of the external plates (Plates 1 and 4) to limit the displacement of the internal plates (Plates 2 and 3) during operation. This is a simplification in relation to the experimental test carried out by Martins (2020) since in his case the external plates that do not suffer pressure loading can also deform.

It is important to mention that there is no difference between contact models that allow sliding in the corrugation because the outer plates are modeled as fixed and drastically reduce how much the center plates can slide during loading. It was opted to use the frictionless contact condition to represent the contact between the plates since this model was used by Nascimento (2013) and Donati (2019) and no significative variations on the results were found between this configuration and the rough contact configuration.

In all, three frictionless contact conditions were modeled: between the external surfaces of plates 1 and 2, between the internal surfaces of plates 2 and 3 and between the external surfaces of plates 3 and 4.

The prescribed pressure loading condition was applied to the internal surfaces of the internal plates (Plates 2 and 3).

Table 7 – PSHEs pressure loading boundary condition.

Type of Condition	**Name/Value**	**Surfaces**
Contact	Bounded	Surfaces in contact between welds and plates
	Frictionless	Surfaces in contact between plates
Solid Restrictions	Fixed Support	All external plate's surfaces (Plates 1 and 4)
Internal Pressure	Prescribed Pressure (0.8, 1, 1.2, 1.4 e 1.6 MPa)	All central plate's internal surfaces (Plates 2 and 3)

Source: Author (2021)

Figure 30 – PSHE geometric configuration

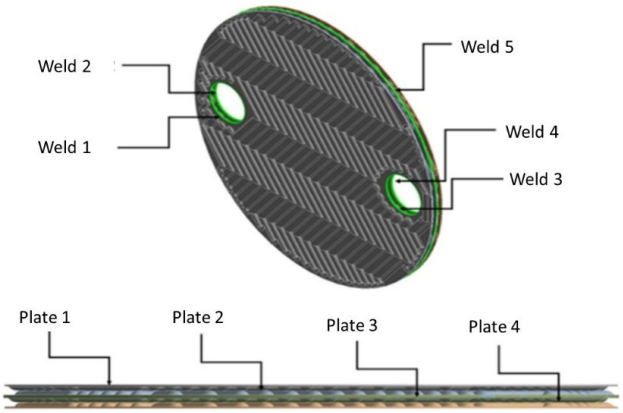

Source: Author (2021)

4.3 MESH AND REFINEMENT TEST

The mesh was generated using the adaptative size function with tetrahedral elements for the plate and hexahedral elements for the welds. Three face sizing controls were created, two for the internal and external plates, respectively, and one for the weld's surfaces. All face sizing was set with a hard behavior, preventing the creation of elements with a length greater than that determined. All mesh refinement tests were performed with the 1.4 MPa pressure loading using only half of the plate, since it is symmetrical. Table 8 presents the mesh refinement test for the PSHE geometry, showing the number of elements, nodes and face sizing controls. The max stress values and contact force results were used to compare meshes' efficiency to better represent the structural behavior. The simulation time and the memory used for the simulation were used to compare the computational cost. The workstation's configuration used for the mesh refinement test is:

- Processor: Intel® Core ™ i7-7700 CPU @3.60 GHz
- Memory (RAM): 32 GB

Beyond mesh 4 all cases were made using a cluster due to the excessive memory necessity for the cases. The cluster have the following configuration:

- Processor: Xeon
- Memory (RAM): 128 GB

Table 8 – Mesh refinement test for the PSHE geometry

Mesh	1	2	3	4	5	6
Elements	371902	629165	988286	1930999	3316078	7567630
Nodes	802992	1313148	2030529	3792925	6442971	13756428
Element size of inner plates [mm]	1.5	1.25	1	0.75	0.75	0.5
Weld's element size [mm]	0.5	0.4	0.3	0.25	0.2	0.2
Element size of outer plates [mm]	3	2.5	2	1.5	0.75	0.5
Max Stress [MPa]	584.33	320.47	364.09	408.21	463.15	457.16
Contact force [N]	1162.6	1323.2	1364	1589.1	1658.6	1435.9
Simulation time [Hour]	1.35	3.33	18.05	36.5	12.08	53.14
Memory Used [GB]	13.575	14.552	17.536	31.643	50.731	106.69

Source: Author (2021)

The memory used and the total time of the simulation increased exponentially with the increase of the mesh's number of elements. More refined meshes than mesh 4 exceeded the RAM limit of the workstation, therefore the cluster was used.

It can be seen that between meshes 1 and 2 the maximum stress decreases drastically, indicating that mesh 1 is so rough that it affects the stress field in the plate. For the other meshes, the increase in refining showed a more linear behavior for the maximum stress. For the strength, the increase in refining tends to increase significantly, with a variation between meshes 1 and 4 of about 400 N.

As commented before, mesh 1 has the higher error, mainly in the max stress. Beyond mesh 1, the behavior of the stress error curve tends to attenuate, however, it can't be said that mesh 4 is sufficiently refined to represent the stress behavior, since the error variation between meshes 3 and 4 is about 5%. All results shown in the next chapter were based on mesh 4.

As for the force error behavior, the increase of the refinement drastically reduces the error, but differently from the stress error curve, this curve doesn't attenuate. This behavior can be associated with the difference in the inner and outer plates element size, since for the outer plate, the element size reduction was from 3 to 1,5 mm, and for the inner plate it was reduced from 1,5 to 0,75 mm. Figure 31 shows the mesh configuration in the geometry.

Figure 31 - Mesh configuration in the plates and the welds.

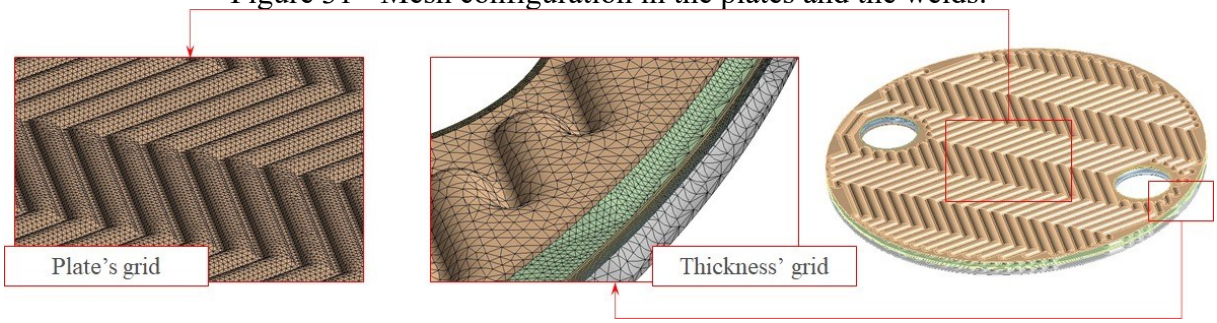

Source: Author (2021)

5 RESULTS AND DISCUSSIONS

5.1 MODEL VALIDATION

5.1.1 PSHE PRESSURE LOADING

In this section the focus will be on comparing the results obtained through numerical models with the stress measurement points obtained by means of strain gauges presented in Martins (2020). Table 9 and Table 10 present the von Misses Stress in different regions of the plate for models with simple (welds and material base applied the same properties) and complex welding (weld applied differnt properties), respectively.

All points analyzed had an increase in von Mises stress as a result of the increase in pressure. Even if the maximum stress in the plate is much higher than the yield stress of the material, it can be seen that the mean stress in the corrugation hardly reaches values above 25 MPa. For the welds, it can be observed that the port's have a very low stress in relation to the external, and that none of the regions presented a stress above the yield limit of the material. Also results for the maximum and average von Mises stress with the simple and complex model for the weld have little difference indicating that the use of the same material properties for the plate and the weld region is a good approximation for mechanical stress estimation, since none of the models include weld defects conditions.

Table 9 - Von Mises stress in the simple weld model

Von Mises Stress [MPa]		**Pressure [MPa]**				
		0.8	**1**	**1.2**	**1.4**	**1.6**
Plate's Maximum [MPa]		232.63	290.43	342.31	385.75	424.28
Plate's Average [MPa]		13.53	12.69	19.77	22.88	25.96
Weld's Maximum	**External [MPa]**	83.17	101.11	117.93	133.82	149.13
	Upper Port [MPa]	36.79	47.16	57.96	69.13	80.70
	Lower Port [MPa]	36.44	46.66	57.31	68.21	79.48

Source: Author (2021)

Table 10 - Von Misses stress in the complex weld model

Von Mises Stress [MPa]		Pressure [MPa]				
		0.8	**1**	**1.2**	**1.4**	**1.6**
Plate's Maximum [MPa]		231.66	289.13	340.93	384.51	422.69
Plate's Average [MPa]		12.22	15.20	18.15	21.10	24.03
Weld's Maximum	**External [MPa]**	86.29	104.65	122.04	138.6	154.51
	Upper Port [MPa]	38.538	47.147	55.416	63.506	71.49
	Lower Port [MPa]	34.71	42.80	50.91	59.07	67.07

Source: Author (2021)

It can be seen that along the plate, the average stress is between 10 MPa and 30 MPa, having values in the inlet (upper port) and outlet (lower port) regions between 40 and 80 MPa. This could indicate that the possible cause of failures in the plates is due to defects during the welding process, since the average stress values in this region are below the yield limit of the material. It is possible to observe that a higher stress values for this region were found around the perimeter of the plate (external), between the junction of the plates and the weld ring geometry, close to the external weld.

Figure 32 presents the stress field for 1 MPa pressure loading for the PSHE plates with the complex weld's model, respectively, with the indication of the point of maximum and minimum von Mises stress. The same behavior seen by Nascimento (2013) can be seen in the contact point area, in which the geometry presents stress peaks in the contact region along the channels, having values higher than 200 MPa for the peaks. This behavior was also seen in Hyun-Seok, Jong-Rae and Seung-Hun (2020). It is important to mention that in the latter work, the behavior in the contact region is evaluated in the elastic-plastic regime, with lower peak values even though the load is ten times greater. Stress plots for the other pressure conditions analyzed are similar and not shown here.

Figure 32 – PSHE plate's von Misses stress field for 1 MPa pressure loading - Complex Weld Model. Units are in MPa.

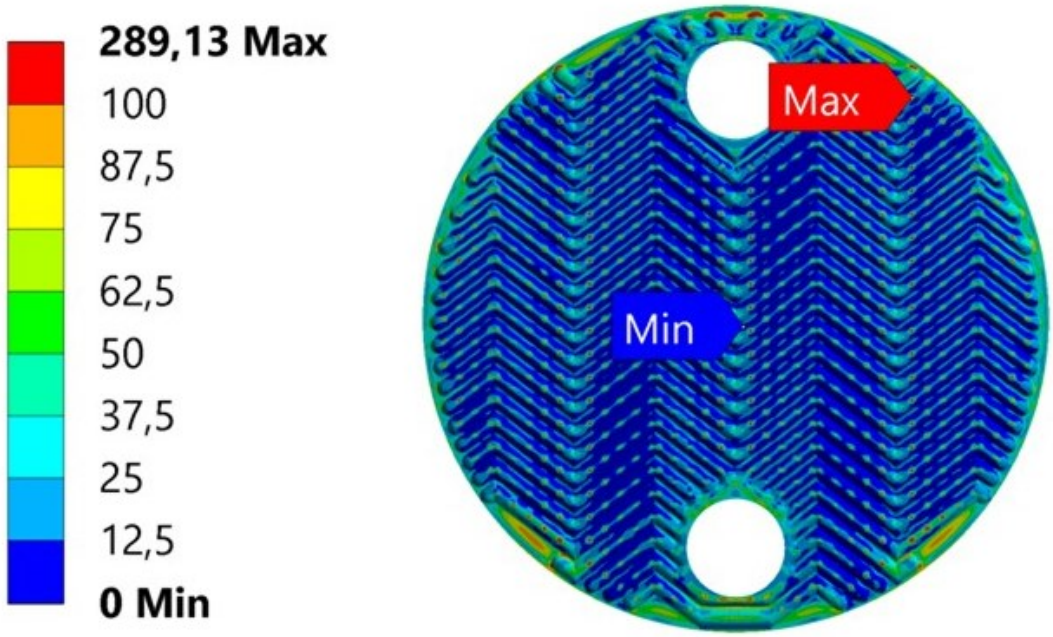

Source: Author (2021)

In order to compare the stress measurements points analyzed by Martins (2020), the same points were highlighted in Table 11 and Table 12, for the simple and complex weld models, respectively. For all pressure loads, points between 3 and 10 had the smallest error when compared to experimental tests. Figure 33 shows the measurement points.

Figure 33 – Measurement Points.

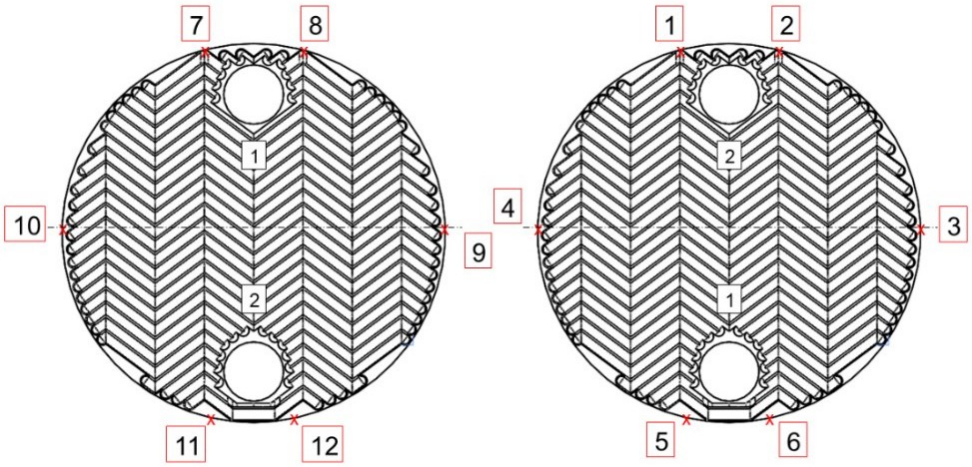

Source: Author (2021)

For the other points (1, 2, 11 and 12), the error is greater than 25%, reaching values of up to 80%. It is important to note that these points may have greater difference between numerical and experimental results because they are located in a region of the plate in which the agreement between the real plate and the numerical modeled geometry is lower (see red squares indicated in Figure 34). Other source of error for this region is the material properties for the weld. Since only average values for the weld properties material have been considered, and the weld geometry has been simplified as a square cross section rim, they can be distorting the stress field in this region. It is interesting to highlight here that points 1 and 12; 2 and 11; 3 and 10; 4 and 9; 5 and 8; 6 and 7 are equivalent due to the position and symmetry of the geometry.

Figure 34 - Complex dimple region in the real plate.

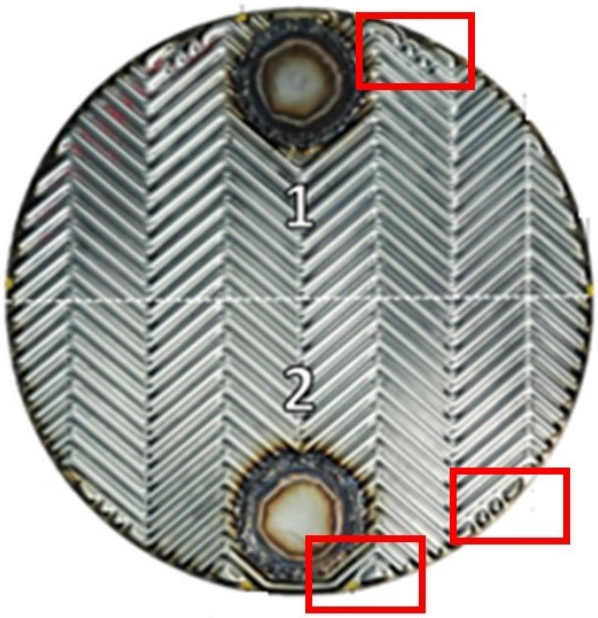

Source: Adapted from Martins (2020)

Table 11 – Measurements Results: Numerical and Experimental - Simple Weld Model.

Pressure Point	1 MPa			1.2 MPa			1.4 MPa		
	Numerical [MPa]	Experimental [MPa]	Error (%)	Numerical [MPa]	Experimental [MPa]	Error (%)	Numerical [MPa]	Experimental [MPa]	Error (%)
1	27.80	12.48	55%	32.64	13.20	60%	37.59	13.76	63%
2	67.56	114.18	-69%	79.87	138.47	-73%	92.15	163.84	-78%
3	76.34	89.63	-17%	90.05	95.10	-6%	103.75	101.04	3%
4	91.70	113.52	-24%	110.12	120.78	-10%	128.53	128.29	0%
5	11.40	12.08	-6%	12.10	13.78	-14%	12.82	13.99	-9%
6	62.44	67.61	-8%	72.39	73.94	-2%	81.95	80.54	2%
7	118.05	113.16	4%	140.74	136.78	3%	163.29	160.68	2%
8	74.71	65.53	12%	86.27	85.15	1%	97.77	96.18	2%
9	17.64	11.47	35%	21.11	12.70	40%	24.63	31.25	-27%
10	21.31	27.43	-29%	26.46	29.46	-11%	31.66	31.25	1%
11	66.44	122.37	-84%	78.97	141.60	-79%	91.49	162.29	-77%
12	67.70	98.20	-45%	80.21	108.75	-36%	92.75	120.23	-30%

Source: Author (2021) – Experimental data adapted from Martins (2020)

Table 12 – Measurements Results: Numerical and Experimental - Complex Weld Model.

Pressure	1 MPa			1.2 MPa			1.4 MPa		
Point	Numerical [MPa]	Experimental [MPa]	Error (%)	Numerical [MPa]	Experimental [MPa]	Error (%)	Numerical [MPa]	Experimental [MPa]	Error (%)
1	27.45	12.48	55%	32.48	13.20	59%	37.30	13.76	63%
2	68.37	114.18	-67%	78.98	138.47	-75%	91.15	163.84	-80%
3	77.30	89.63	-16%	88.34	95.10	-8%	101.79	101.04	1%
4	103.45	113.52	-10%	107.70	120.78	-12%	125.74	128.29	-2%
5	12.91	12.08	6%	12.51	13.78	-10%	13.31	13.99	-5%
6	67.52	67.61	0%	71.16	73.94	-4%	80.54	80.54	0%
7	113.93	113.16	1%	137.93	136.78	1%	160.09	160.68	0%
8	65.42	65.53	0%	84.52	85.15	-1%	95.81	96.18	0%
9	11.28	11.47	-2%	20.96	12.70	39%	32.97	31.25	5%
10	27.48	27.43	0%	26.06	29.46	-13%	31.15	31.25	0%
11	77.49	122.37	-58%	78.23	141.60	-81%	90.65	162.29	-79%
12	78.08	98.20	-26%	79.31	108.75	-37%	91.73	120.23	-31%

Source: Author (2021) – Experimental data adapted from Martins (2020)

It is important to note that the plate has highly complex dimples in the region with the biggest differences and as these regions have been simplified as flat, it may have a great impact on the stress and displacement field. The dimples can be seen in Figure 34. One way to better see the effect of the dimple's nonexistence is by analyzing the displacement field along the plate, as seen in Figure 35, where the displacement has a higher value in the region where the dimples were simplified, condition that does not happen in the real plate.

Can also be seen that the same behavior of Nascimento (2013) about the average displacement of a plate is also seen here, having the most influence from the corrugation of the plate, this behavior was expected since the plate should move almost uniformly along the pack of plates. In the other hand, the area of the inlet and outlet ports has zero displacement, since these surfaces remain in contact (bounded contact) with the other plate port's surfaces of the pair.

Figure 35 – Displacement field for 1.4 MPa pressure loading. Units are in mm.

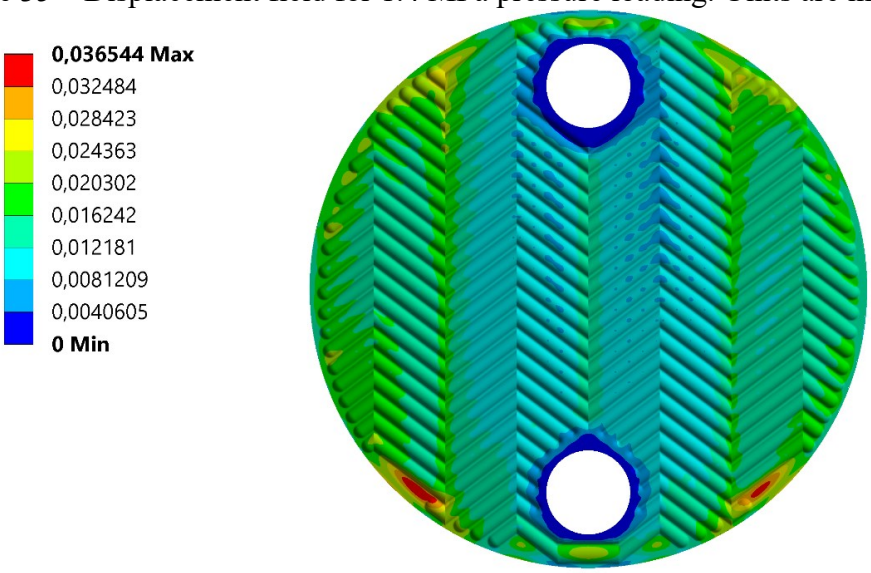

Source: Author (2021)

5.1.2 PSHE FATIGUE BEHAVIOR

For the estimation of the alternating stress for fatigue analysis a von Misses stress value is necessary. Since the exact location of the weld failure region found by Martins (2020) was not specified and knowing that the stress point 2, presented in the measurements results (Table 11 and Table 12), was used for the fatigue analysis in the work of Martins (2020), the maximum equivalent mechanical stress range ($\Delta S_{p,k}$) found in the weld region for the numerical

model will be used in instead, since point 2 has a high numerical error (67 – 80%). This implies using the maximum stress region of the weld for fatigue analysis in numerical cases instead of the maximum stress using strain gauges in Martins (2020). The maximum stress region analyzed is shown in Figure 36 and the comparison between the stress values used in Martins (2020) and the cases with simple and complex welds are shown in Table 13 – Von Misses stress values used in fatigue analysis for the experimental work of Martins (2020) and the numerical model.Table 13.

Figure 36 – Maximum equivalent stress value at the weld for the numerical model.

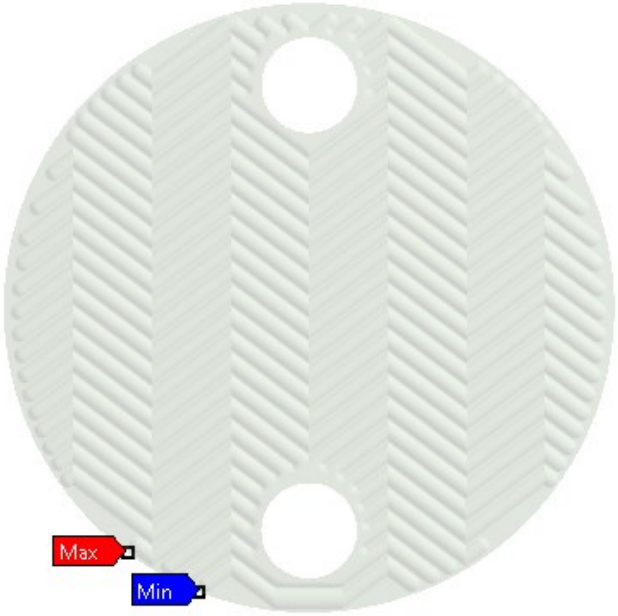

Source: Author (2021)

Using the maximum stress value estimated by the numerical model from the weld implies in a difference from 8.92 to 15.4% between the complex weld model and experimental results. For the simple weld model, the difference is from 11.45 to 18.32%. The comparison between the two numerical models indicates that the peak stress value found in the weld is not greater than 3.57%, this implies that simplifying the model considering only the base material does not have such a significant effect for the numerical model when trying to estimate the stress level. This was already expected, since the use of different materials for welding does not consider the heated affected zone and discontinuities that generate cracks and stress concentrators, as mentioned before. Notice that the maximum stress found in the weld region for the numerical model is not coincident with the same position for the experimental work of

Martins (2020). However as indicated above, the values estimated in the weld region do not differs more than 20% between numerical and experimental results. Since the fatigue analysis should be estimated with the maximum stress values, these results were used to estimate the alternating stress for fatigue life considering they are in the weld region, not is the exact same position.

Table 13 – Von Misses stress values used in fatigue analysis for the experimental work of Martins (2020) and the numerical model.

Pressure [MPa]	**Experimental [MPa]**	**Simple Weld [MPa]**	**Difference – Simple Weld [%] – experimental data**	**Complex Weld [MPa]**	**Difference – Complex Weld [%] – experimental data**	**Difference between numerical models [%]**
1	114.18	101.11	11.45	104.63	8.35	3.48
1.2	138.47	117.93	14.83	122.04	11.87	3.48
1.4	163.84	133.82	18.32	138.6	15.41	3.57

Source: Author (2021) – experimental data from Martins (2020)

Table 14 presents the results obtained by Martins (2020) using experimental tests and ASME VIII DIV 2 to estimate the lifetime of the plates, and the life time obtained using the numerical approach for simple and complex weld models. All numerical cases were carried out using the maximum alternating stress curves of the materials up to 99000 cycles shown in Figure 29 since the expected life is in low cycle fatigue. It is important to mention that this table only shows the results for the Gerber fatigue failure criterion. The same tests were performed for simple and complex welding cases using the criteria of Goodman and Soderberg, and can be found in APPENDICES I, II and III. The material properties applied in Martins (2020) for the estimation of the k_f were the same applied here as material base for the simple and complex weld model.

It can be seen that all results for k_f equals to 1 have the maximum lifetime of 99000 cycles. This indicate that this load, without discontinuities in the material or weld wouldn't be enough for the base material to fail at this range. To obtain expected infinite life for this case the alternating stress curve should be expanded to 10^6 cycles.

As noted by Martins (2020), k_f values proposed by ASME (1 to 4) are not enough to represent the life of the plate in virtue of the weld, tests using k_f equals to 5, 5.9 and 6.2 were

carried out. Differently from what was observed by Martins (2020) by the ASME standard, the numerical model indicated that for k_f between 5.9 and 6.2 the predicted life expectancy was much lower than that observed experimentally for both numerical models for the operating pressure of 1.2 and 1.4 MPa, with the model with simplified welding having the lowest values. However for operating pressure of 1 MPa the simple weld model indicated that the predicted life with k_f equal to 5.9 was close to the experimental one. The difference between the numerical models reached values of up to 25% and the model with k_f equal to 5 estimating better life considering the complex weld, with deviations between 10.4% and 3% to the experimental results. Notice that results of fatigue life with k_f equal to 5 are not available in the experimental data.

Table 14 - Fatigue strength reduction factor (k_f) effect in the lifetime of the plates.

Pressure [MPa]	**Number of Cycles (Experimental) – Martins (2020)**	k_f	**Number of Cycles (ASME VIII DIV 2) – Martins (2020)**	**Number of Cycles - ANSYS (Complex Weld)**	**Number of Cycles - ANSYS (Simple Weld)**
1	14059	1	1000000	99900	99900
		2	1000000	99900	99900
		3	182420	99900	99900
		4	55933	66023	55933
		5	-	15519	22140
		5.9	13509	7057	13509
		6.2	10825	4955	10825
1.2	8562	1	1000000	99900	99900
		2	579875	99900	99900
		3	79659	99900	99900
		4	26860	25999	32160
		5	-	7198	9774
		5.9	13509	2813	3447
		6.2	5594	1987	2447
1.4	3167	1	100000	99900	99900
		2	228564	99900	99900
		3	42353	60862	75832
		4	14821	19593	15218
		5	-	3263	4197
		5.9	7014	1317	1620
		6.2	3122	0	1145

Source: Author (2021)

It is important to note that even if the stress level between the numerical models is very close, the deviation found for life is still high, indicating that the choice of the set of mechanical properties, fatigue life model and k_f must be selected very carefully, and should be done, if

possible, with some kind of experimental validation. The choice in the fatigue failure criterion can cause even more deviations depending on whether the model is more or less conservative.

Figure 37 presents the estimated life for complex and simple weld models with the ideal fatigue strength reduction factor (k_f) for each fatigue failure criterion. As previously presented, the complex weld model represents the curve closest to that obtained experimentally and both models showed greater deviations for lower operating pressures, mainly for the Soderberg criterion.

Figure 37 - Estimated life for the complex and simple weld models with best fit fatigue strength reduction factor (k_f) for Soderberg, Goodman and Gerber criteria.

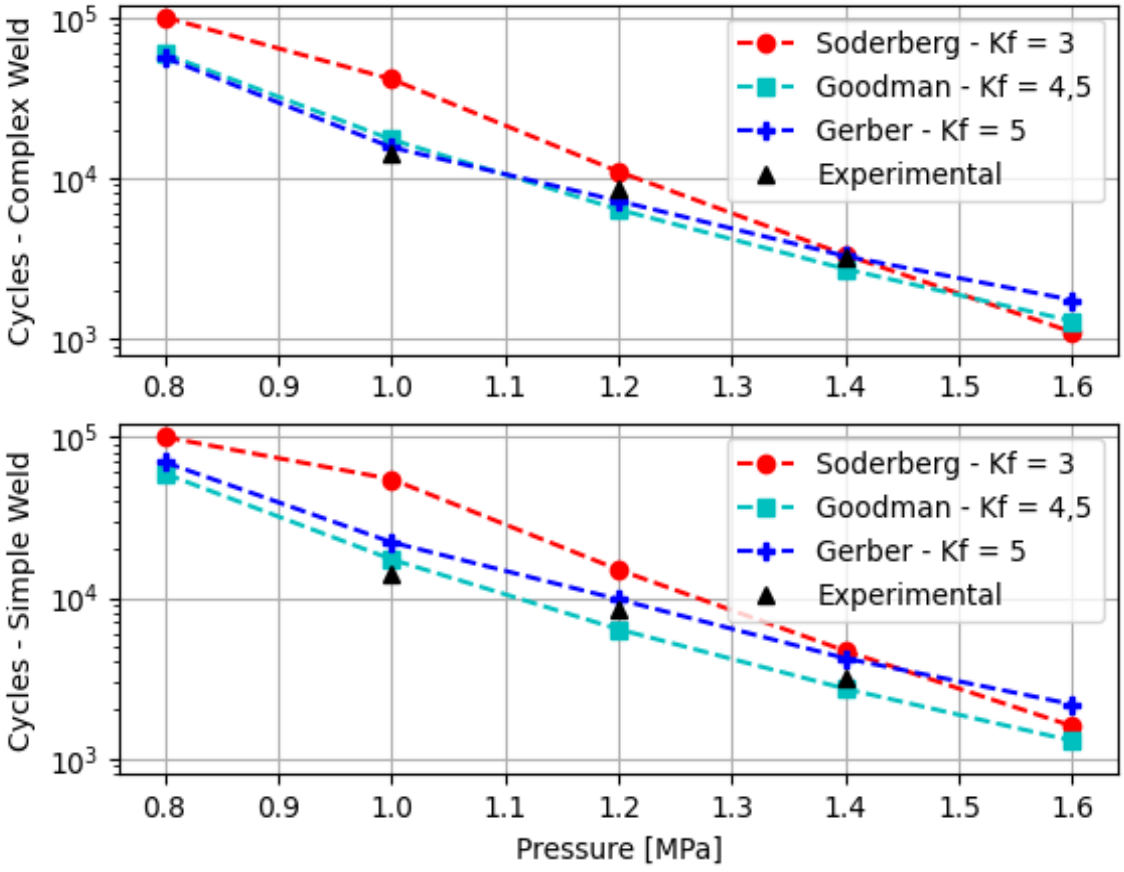

Source: Author (2021) – experimental data from Martins (2020)

Figure 38 presents the lifetime along the channels for the 1.4 MPa pressure loading with a fatigue strength reduction factor (k_f) equals to 6.2 and Gerber failure criterion. Results were obtain through the ANSYS fatigue tool, that applies the same methodology presented in section 3.2 but locally. It can be seen that the contact region and regions without the dimples

have lower lifetimes. Since the contact points are expected to suffer a plastic strains and the fatigue analysis can be only carried out in the elastic regime, the life in these points are zero.

Can also be seen that the port region presented lower life values when compared with the corrugation. This was expected since this region is in contact with the other plate, even though it does not suffer plastic strain.

Figure 38 – Plate's lifetime for the 1,4 MPa pressure loading with k_f equals to 6.2.

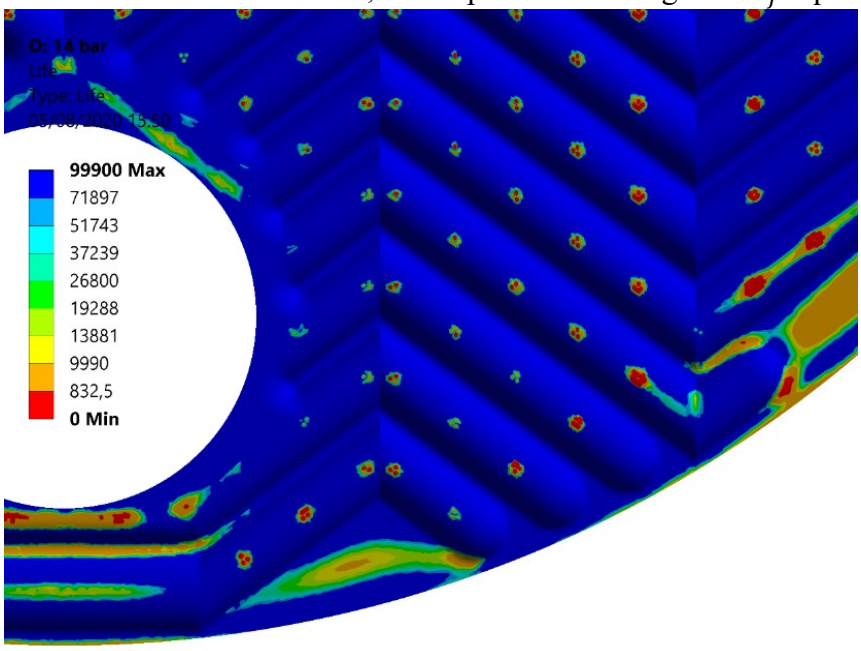

Source: Author (2021)

5.2 CONTACT BEHAVIOR

To have a better understanding of the contact region, an arbitrary contact point was selected, and the stress field in its region analyzed, as shown in Figure 39. For 1 MPa pressure loading, it can be seen that most of the region is below the Tensile Yield limit (170 MPa) but there is still a part that suffers plastic strain, having a maximum stress value of 253.55 MPa. For 1,4 MPa the same behavior can be seen, but with a higher stress value of 341.23 MPa. It is important to note that the plastic strain only occurs in the sliding portion of the contact area, as shown in Figure 40. Both cases presented secondary peak stresses with lower stress intensities.

To verify the real behavior of the stress field along the contact area, the ideal would be to perform the same analysis proposed by Lee and Lee (2014), using a plasticity model like isotropic bilinear or multilinear plasticity models.

Figure 39 – Von Misses stress in on an arbitrary contact point: (a) 1 MPa. (b) 1.4 MPa.

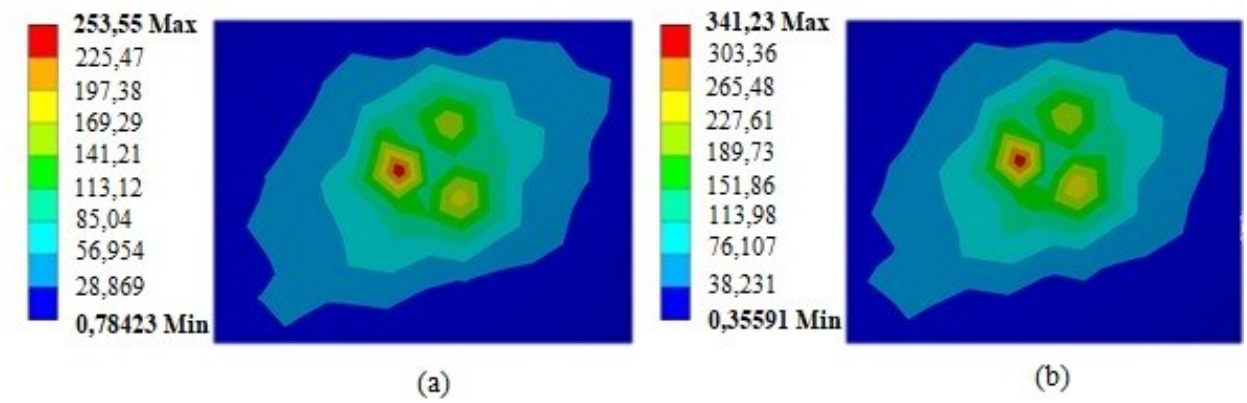

Source: Author (2021)

Figure 40 – Contact area behavior

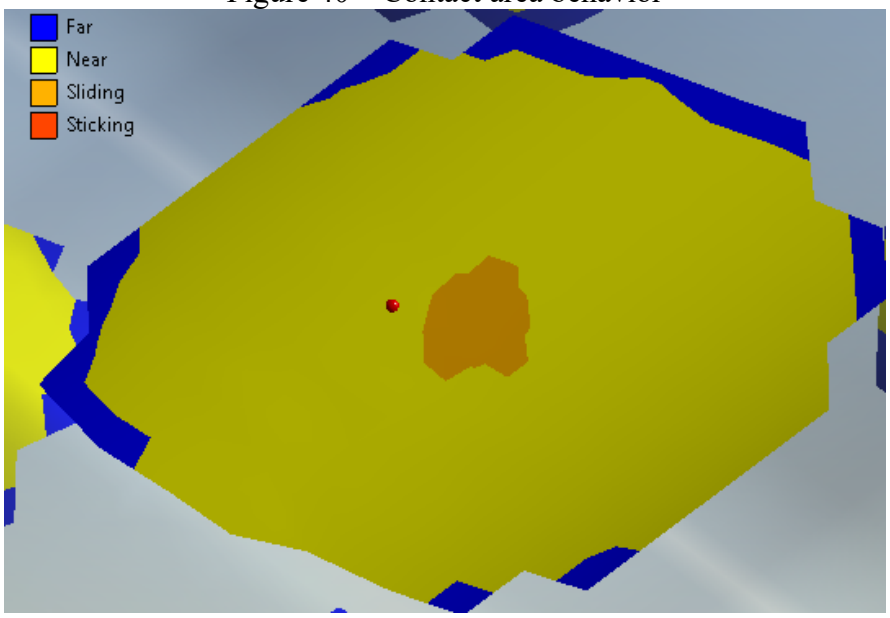

Source: Author (2021)

In order to have a better understanding of the von Mises equivalent stress behavior along the top of the channel, the stresses were obtained for the paths A, B and C, as shown in Figure 41. Figure 42 presents the von Mises equivalent stress along the top of the channels for 1.4 MPa pressure loading in paths A, B and C.

Figure 41 – Positon of each path

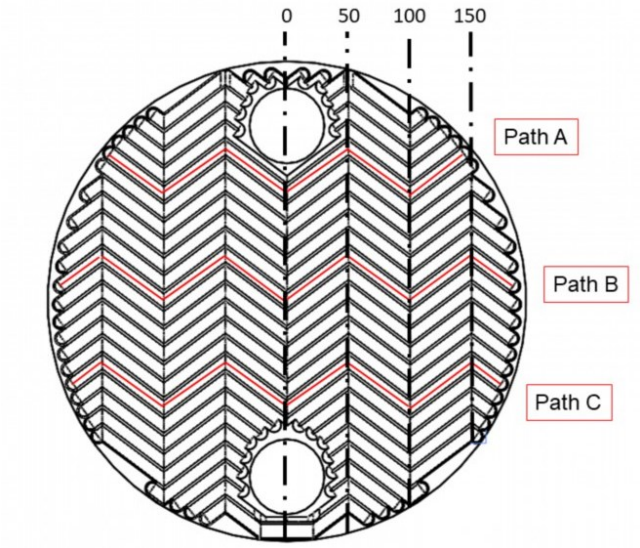

Source: Author (2021)

Figure 42 – Von Mises equivalent stress along the top of the channels with 1.4 MPa pressure loading.

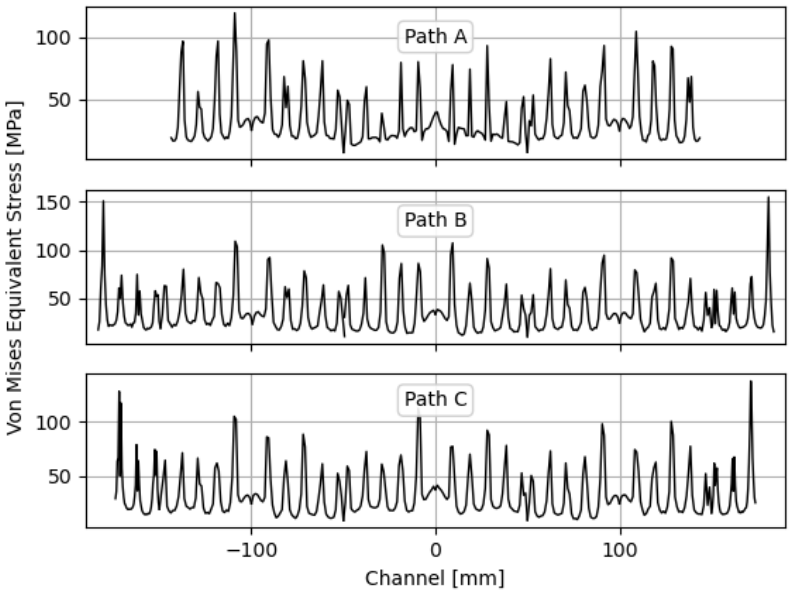

Source: Author (2021)

It can be seen that for the points outside the contact area, the average stress is around 25 MPa while peak values reach over 50 MPa. Paths B and C have higher peak values on the sides, reaching 100 MPa. Path A have more stress peaks close to 100 MPa limit when compared with the other paths, indicating that the contact force between plates is not well distributed along the plate. It also can be seen that the peak stresses are no near the value of 341.23 MPa. This

occurs because the contact point is slightly off-centered, reducing the maximum peak values found along the top of the corrugation channel.

The points with the change of direction of the channel -100, 0 and 100 have lower stress peaks when compared with points -150, -50, 50 and 150. This could indicate that the direction of the corrugation's zig-zag have influence in the rigidity of the plate in that region.

Figure 43 presents the contact force between the central plate. This force was obtained using ANSYS contact tool by integrating the force along all the contact points sliding area of the plates 2 and 3 (Figure 40). The behavior of the curve can be obtained by the linear equation $F = 2265.47P$, having a determination coefficient (R^2) equals to 0.9566.

For the 1.4 pressure loading, the force was 3.33 kN, showing that the contact forces have a high impact in the structural behavior. Two considerations must be made regarding this result, since the external plates (1 and 4) are totally fixed, the central plates (2 and 3) can not separate, a condition observed by Martins (2020) and which has a significant effect on life behavior in fatigue, even more including the tightening of the plates. The other is in relation to the type of contact used, as the slip is free without any type of lateral restriction, the use of contacts with friction can alter the structural behavior of the plate.

Figure 43 – Contact force between the central plates.

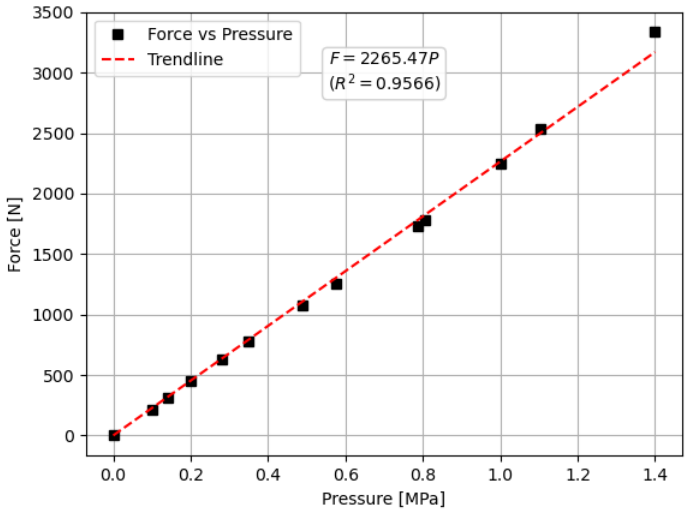

Source: Author (2021)

In order to evaluate the behavior of the plates in a real-life condition, the prescribed pressure loading was used in addition to the boundary conditions presented in Table 7, with the same pressure in the external surfaces of plates 2 and 3 (internal and external channels pressure load condition) The influence of the external load was analyzed isolated and in addition to the

internal load. It is important to note that this condition has not been studied by Martins (2020), therefore, there are no experimental data to validate this result.

Figure 44 shows the stress field for 1.4 bar pressure loading conditions. Firstly, it can be seen that when the pressure is applied only in the external surfaces of plates 2 and 3 (central plates) the stress field reaches higher values when compared to the case with prescribed pressure only on the internal surfaces and mainly in the contacts points, in the inlet and outlet ports. For the case with internal and external pressures, the stress intensity reduces drastically, with the maximum value in the corrugation reaching 15 MPa.

Figure 44 – Stress Field: (a) Internal Load. (b) External Load. (c) Internal and External Load.

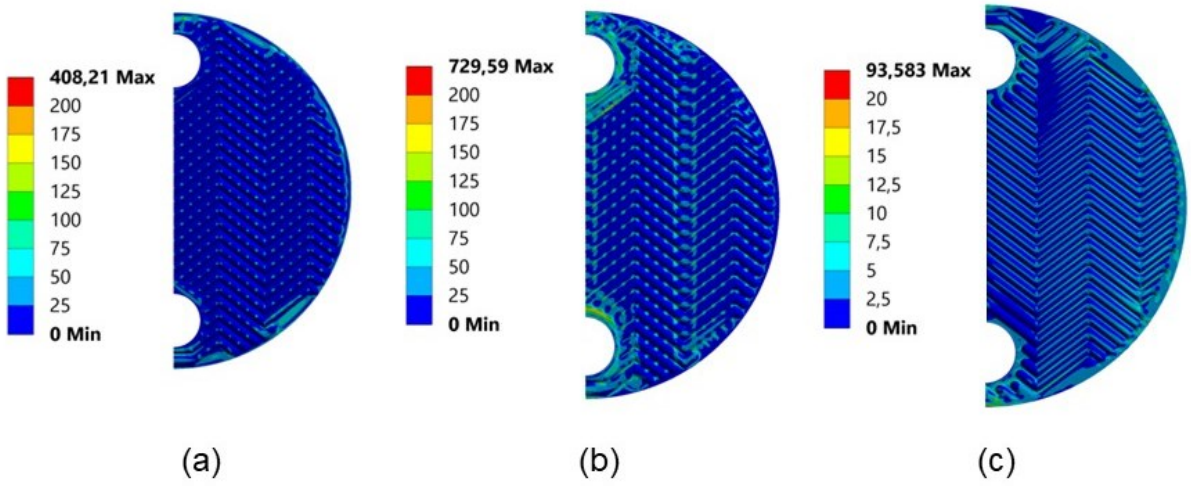

Source: Author (2021)

Figure 45 shows the contact region for the cases mentioned above. As mentioned before, the internal pressure tends to induce a contact between the internal and external plates, slightly off-centered of the top of the corrugation and with three stress peak values, being two of them secondary. In other hand, the external load tends to induce a contact region between the internal plates, having only one peak stress in the center of the contact point. For the case with both pressures, it can be seen that the stress field varies, mainly in the contact region, without presenting well-defined contact points. This indicates that if the pressure load in the external and internal channels are equal, contact between the plate corrugation region reduces.

Figure 45 – Contact Region: (a) Internal Load. (b) External Load. (c) Internal and External Load.

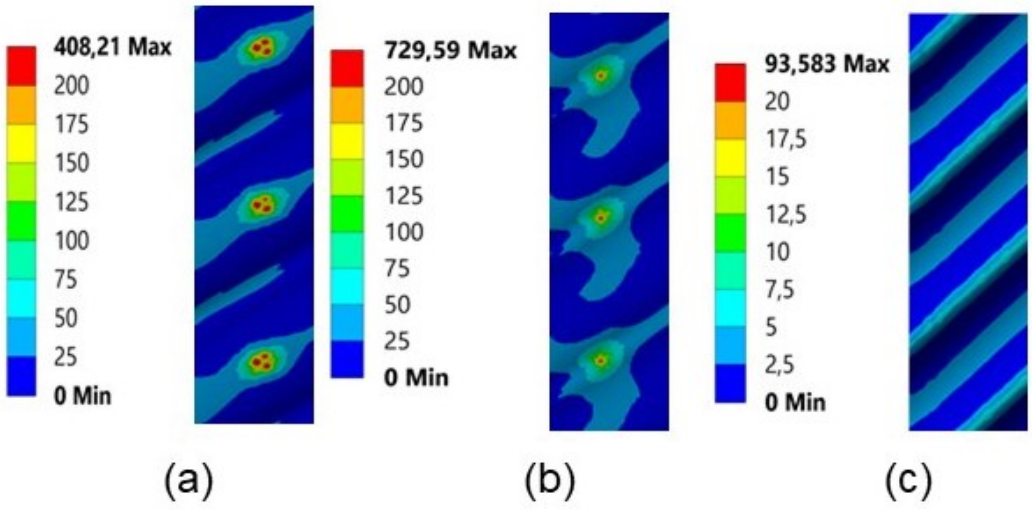

Source: Author (2021)

It is important to note that this does not represent a real operation condition since during operation, the pressure loading in a channel suffer the effect of pressure dropping, and since the flow in the exchanger may occurs in a counterflow way. This behavior would result in a variation in the intensity of stress at the contact points along the direction of the entry and exit ports. Having a greater intensity in the highest region of the corrugation close to the entrance, and moving to the lowest region of the corrugation as the flow approaches the exit. As this behavior was not observed, it would be necessary to conduct a case using fluid-structural analysis to take the pressure drop into account.

6 CONCLUSIONS

In this work finite element analysis was conducted in a Plate and Shell heat exchanger under hydrostatic pressure loading inside the plates, in order to evaluate the stress field in the exchanger. Once the stress field was obtained, numerical fatigue analysis was conducted with multiple fatigue reduction factors to evaluate the plate's life under a repeated load. The results were compared with experimental tests previously published.

For the von Mises Stress Field, 4 of 12 measurement points obtained by Martins (2020) had an error in relation to the experimental analysis greater than 20%. These 4 points were located at a region of the plate in which the numerical geometry is highly distorted in relation with the real plate's geometry. These points are also close to the welds, and since the weld was simplified without the heat affected zone and with simplified square cross section, material properties variations could influence in the measurements. The configuration with different material for the weld did not show significant variations for the stress field along this region.

Due to simplifications in geometry, high displacements were found at flat points close to experimental measurement points. This was the main reason for the high error for the same points when analyzing the stress values.

For the fatigue analysis, since stress measurement point used in the experimental analysis had a high error due to geometric differences, the maximum stress found in the weld's region was used in instead. This implies in a difference of 15% between the experimental and the numerical mechanical stresses used to evaluate the alternated stress. Multiple fatigue reduction factors were used to take in consideration. Just like Martins (2020), the ideal value to obtain the expected life is 5 for Gerber criteria. It was concluded that the use of a material different from the base material for the weld does not have a significant effect on the fatigue analysis, having a greater influence of the fatigue life reduction factor, which also covers the weld region. The ideal fatigue life reduction factor to represent the weld behavior was estimated for the Goodman, Sodeberg and Gerber failure criteria, with greater deviations for low pressures.

As for the contact point, the yield stress was exceeded in the sliding portion of the contact area, with the max stress slightly off-centered with the top of the corrugation. It could also be seen that because in the contact points region occurred a plastic strain, this region also failed in the fatigue analysis.

Two secondary peaks were also found with lower stress intensities. In order to obtain the real stress field in this region it would be necessary to use a plasticity model, such as a multilinear hardening model. The stress field in the top of the corrugation in different corrugation paths was also obtained, showing that the mean stress along the paths and the stress in the contact points varies in the direction of the inlet and outlet ports. This behavior can be associated with a variation of the plate's rigidity as a function of the chevron angle and the direction where the "V" of the corrugation points. This could also indicate that even though the pressure loading is uniformly distributed in the plate's surface, the contact force is not uniformly distributed as well. The same behavior of high stress values in the contact area and the mean displacement value for the plate seen by Nascimento (2013) were also found on this work.

The mean force between the central plates was also evaluated using the contact tool provided by ANSYS. Since this effect was not validated with experimental tests it is considered a preliminary analysis. Regardless of that, it can be seen that the contact force is linear dependent of the pressure, and for 1.4 MPa the force exceeds 3 kN. This indicates that the contact between plates has a big influence in the structural integrity of the plates. It is also important to mention that since the external plates were modeled as fixed supports, therefore, not deforming or having a displacement, the internal plates does not separate. This could have a significant effect in the force between plates.

The use of loading in the two exchanger channels suggests that when the loads are applied simultaneously, they tend to reduce the stress state in the plate, while loading in only one of the channels tends to drastically increase the level of stresses in the contact region.

At this point it is important to list all the divergences between the numerical and the experimental tests in order to know how representative the numerical model can be and in which conditions it diverges from the experimental and operation conditions:

- Simplifying plate's material as isotropic;
- Disregarding plasticity effects;
- Contact behavior as frictionless;
- Evaluating only internal pressure;
- Disregarding heat affected zone mechanical properties variation;
- Simplifying the external plates as fixed supports;

- Simplifying welds as rims with different properties in relation with the base material.

Even with all these simplifications, the von Mises Equivalent Stress was obtained with an error between 0 and 20% for the majority of the measurement's points. The stress in the contact point and in the top of different corrugation's paths were evaluated, also obtaining the contact force between central plates. The fatigue life was also estimated with an error between 8 and 15% depending of the load for the same failure region, reaching all the objectives proposed in this work.

Based on the conclusions drawn, suggestions were made for future work:

- Evaluate the number of plates to represent the pack;
- Use a plasticity model to evaluate the real stress field in the contact region;
- Use an orthotropic linear model to evaluate the difference in the elasticity model in different directions of the plate;
- Evaluate the separation of the plates during operation with internal and external loadings;
- Compare the results obtained with the hydrostatic pressure loading with a fluid structure analysis based on hydrodynamic pressure loading.

REFERENCES

ADOLFSSON, Marcus; RASHID, Shivan. **Life Cycle Assessment and Life Cycle Cost of Heat Exchabgers:** A Case for Inter Terminals Sweden AB Located in Port of Gothenburg. 2016. 62 f. Dissertação (Mestrado) - Curso de Chalmers University Of Technology, Chalmers University Of Technology, Chalmers University Of Technology, Gothunburg, 2016.

American Society of Mechanical Engineers. **ASME Boiler and Pressure Vessel Code. Section VIII**: Rules for Construction of Pressure Vessels. Division 2. 2015.

BUDYNAS, Richard G. *et al*. **Shigley's Mechanical Engineering Design**. 10. ed. New York: Mc Graw Hill, 2015.

COOK, Robert D. **Finite Element Modeling for Stress Analysis.** New York: John Wiley & Sons, Inc, 1995. 326 p.

DONATI, Damylle Cristina Xavier. **ANÁLISE NUMÉRICA DA INTERAÇÃO FLUIDO-ESTRUTURA DE TROCADORES DE CALOR DO TIPO PSHE**. 2019. 65 f. TCC (Graduação) - Curso de Engenharia Aeroespacial, Universidade Federal de Santa Catarina, Joinville, 2019.

HYUN-SEOK, Noh; JONG-RAE, Cho; SEUNG-HUN, Song. Plate Pack Structural Integrity Analysis for Plate and Shell Heat Exchangers at High Temperatures and Pressures. **Advances In Mechanical Engineering**, [S.L.], v. 12, n. 2, p. 1-6, fev. 2020. SAGE Publications. http://dx.doi.org/10.1177/1687814019901244.

KAKAÇ, Sadik; LIU, Hongtan; PRAMUANJAROENKIJ, Anchasa. **Heat Exchangers:** Selection, Rating and Thermal Design. 3. ed. New York: Taylor & Francis Group, Llc, 2012. 624 p.

KIM, In Hun; NO, Hee Cheon; LEE, Jeong Ik; JEON, Byong Guk. Thermal hydraulic performance analysis of the printed circuit heat exchanger using a helium test facility and CFD simulations. **Nuclear Engineering And Design**, [s.l.], v. 239, n. 11, p.2399-2408, nov. 2009. Elsevier BV. http://dx.doi.org/10.1016/j.nucengdes.2009.07.005.

LEE, Youho; LEE, Jeong Ik. Structural assessment of intermediate printed circuit heat exchanger for sodium-cooled fast reactor with supercritical CO2 cycle. **Annals Of Nuclear Energy**, [s.l.], v. 73, p.84-95, nov. 2014. Elsevier BV. http://dx.doi.org/10.1016/j.anucene.2014.06.022.

LI, Bin et al. Design and Fatigue Analysis of High Pressure Shell and Plate Heat Exchanger. **Iop Conference Series**: Earth and Environmental Science, [s.l.], v. 233, p.052025-052033, 26 fev. 2019. IOP Publishing. http://dx.doi.org/10.1088/1755-1315/233/5/052025.

HOU, Yaqiong; TANG, Guihua. Thermal-Hydraulic-Structural Analysis and Design Optimization for Micron-Sized Printed Circuit Heat Exchanger. **Journal Of Thermal Science**, [s.l.], v. 28, n. 2, p.252-261, 14 mar. 2019. Springer Nature. http://dx.doi.org/10.1007/s11630-018-1062-8.

MARTINS, Giovani Silveria de Magalhães. **ANÁLISE EXPERIMENTAL DE FADIGA MECÂNICA EM PLACAS DE TROCADORES DE CALOR CASCO E PLACAS.** 2020. 141 f. Dissertação (Mestrado) - Curso de Pós-graduação em Engenharia e Ciências Mecânicas, Universidade Federal de Santa Catarina, Joinville, 2020.

NASCIMENTO, Rafael Sant'Anna do. **ANÁLISE DE COMPORTAMENTO ESTRUTURAL DE PERMUTADORES DE PLACAS.** 2013. 140 f. Dissertação (Mestrado) – Curso de Pós-graduação em Engenharia Mecânica, Universidade Federal do Rio de Janeiro, Rio de Janeiro, 2013.

NORTON, Robert L. **Projeto de Máquinas**\: uma abordagem integrada. 4. ed. Porto Alegre: Bookman, 2013.

PATIL, Rakesh; ANAND, Soham. Thermo-structural fatigue analysis of shell and tube type heat exchanger. **International Journal Of Pressure Vessels And Piping**, [s.l.], v. 155, p.35-42, ago. 2017. Elsevier BV. http://dx.doi.org/10.1016/j.ijpvp.2017.03.004

PELLICCIONE, A.s. et al. Failure analysis of a titanium plate heat exchanger – Mechanical fatigue. **Engineering Failure Analysis**, [s.l.], v. 105, p.1172-1188, nov. 2019. Elsevier BV. http://dx.doi.org/10.1016/j.engfailanal.2019.07.059

SONG, Kee-nam. Structural Behavior Analysis on a Small-scale PCHE Prototype under High-temperature Gas Loop Conditions. **Tech Science Press**, [s.i.], v. 7, n. 4, p.297-305, jan. 2011

SONG, Kee-nam; HONG, Sung-deok. Structural Integrity Evaluation of a Lab-Scale PCHE Prototype under the Test Conditions of HELP. **Science And Technology Of Nuclear Installations**, [s.l.], v. 2013, p.1-7, 2013. Hindawi Limited. http://dx.doi.org/10.1155/2013/520145.

SONG, Kee-nam; HONG, Sung-deok; PARK, Hong-yoon. High-Temperature Structural Analysis of a Small-Scale PHE Prototype under the Test Condition of a Small-Scale Gas Loop. **Science And Technology Of Nuclear Installations**, [s.l.], v. 2012, p.1-10, 2012. Hindawi Limited. http://dx.doi.org/10.1155/2012/312080.

TASCHECK, Bruna Larissa. **NUMERICAL ANALYSIS OF HYDRODYNAMIC CHARACTRRISTICS OF A PLATE AND SHELL HEAT EXCHANGER (PSHE).** 2019. 101 f. Dissertação (Mestrado) - Curso de Programa de Pós-Graduação em Engenharia e Ciências Mecânicas, Universidade Federal de Santa Catarina, Joinville, 2019.

THULUKKANAM, K., Heat exchanger design handbook: Mechanical Engineering. 2. ed. New York: Crc Press, 2013. 1260 p. Disponível em: <https://books.google.com.br/books?id=hmzRBQAAQBAJ&hl=pt-BR&source=gbs_navlinks_s>. Acesso em: 27 fev. 2018.

ZHANG, Lingjie et al. Fluid–structure interaction numerical simulation of thermal performance and mechanical property on plate-fins heat exchanger. **Heat And Mass Transfer**, [s.l.], v. 51, n. 9, p.1337-1353, 4 fev. 2015. Springer Science and Business Media LLC. http://dx.doi.org/10.1007/s00231-015-1507-5.

ZHANG, X et al. PRELIMINARY STRUCTURAL ASSESSMENT OF A PRINTED CIRCUIT HEAT EXCHANGER WITH S-SHAPED FINS. **Nureth: 16.** Chicago, p. 7673-7686. set. 2015.

APPENDIX I - GERBER

Table I 1 - Fatigue strength reduction factor (kf) effect in the lifetime of the plates for 0,8 MPa pressure loading - Complex Weld Model.

Pressure [MPa]	**$\Delta S_{p,k}$ [MPa] (Experimental)**	**$\Delta S_{p,k}$ [MPa] (Numerical)**	**Number of Cycles (Experimental)**	**Kf**	**S_{alt} [MPa] (Experimental)**	**S_{alt} [MPa] (Numerical)**	**Number of Cycles (ASME VIII DIV 2) - Experimental**	**Number of Cycles (Numerical)**
0.8	-	86.29	-	1	-	41.15	-	99900
				2	-	82.29	-	99900
				3	-	123.44	-	99900
				4	-	164.58	-	99900
				5	-	215.72	-	56156
				5.9	-	242.76	-	22118
				6.2	-	255.10	-	15519

Source: Author (2021)

Table I 2 - Fatigue strength reduction factor (kf) effect in the lifetime of the plates for 1 MPa pressure loading - Complex Weld Model.

Pressure [MPa]	**$\Delta S_{p,k}$ [MPa] (Experimental)**	**$\Delta S_{p,k}$ [MPa] (Numerical)**	**Number of Cycles (Experimental)**	**Kf**	**S_{alt} [MPa] (Experimental)**	**S_{alt} [MPa] (Numerical)**	**Number of Cycles (ASME VIII DIV 2) - Experimental**	**Number of Cycles (Numerical)**
1	114.18	104.65	14059	1	57.09	52.33	1000000	99900
				2	114.18	104.65	1000000	99900
				3	171.27	156.98	182420	99900
				4	228.02	209.30	55933	66023
				5	-	261.62	-	15519
				5.9	336.83	308.72	13509	7057
				6.2	353.95	324.41	10825	4955

Source: Author (2021)

Table I 3 - Fatigue strength reduction factor (kf) effect in the lifetime of the plates for 1.2 MPa pressure loading - Complex Weld Model.

Pressure [MPa]	**$\Delta S_{p,k}$ [MPa] (Experimental)**	**$\Delta S_{p,k}$ [MPa] (Numerical)**	**Number of Cycles (Experimental)**	**Kf**	**S_{alt} [MPa] (Experimental)**	**S_{alt} [MPa] (Numerical)**	**Number of Cycles (ASME VIII DIV 2) - Experimental**	**Number of Cycles (Numerical)**
1.2	138.47	122.04	8562	1	69.235	61.02	1000000	99900
				2	138.47	122.04	579875	99900
				3	207.705	183.06	79659	99900
				4	276.94	244.08	26860	25999
				5	-	305.10	-	7198
				5.9	408.48	360.02	13509	2813
				6.2	428.26	389.32	5594	1987

Source: Author (2021)

Table I 4 - Fatigue strength reduction factor (kf) effect in the lifetime of the plates for 1.4 MPa pressure loading - Complex Weld Model.

Pressure [MPa]	**$\Delta S_{p,k}$ [MPa] (Experimental)**	**$\Delta S_{p,k}$ [MPa] (Numerical)**	**Number of Cycles (Experimental)**	**Kf**	**S_{alt} [MPa] (Experimental)**	**S_{alt} [MPa] (Numerical)**	**Number of Cycles (ASME VIII DIV 2) - Experimental**	**Number of Cycles (Numerical)**
1.4	163.8	138.6	3167	1	81.92	69.30	1000000	99900
				2	163.84	138.60	228564	99900
				3	245.84	207.84	42353	60862
				4	327.68	277.20	14821	19593
				5	-	346.50	-	3263
				5.9	483.328	408.87	7014	1317
				6.2	507.9	429.66	3122	0

Source: Author (2021)

Table I 5 - Fatigue strength reduction factor (kf) effect in the lifetime of the plates for 1.6 MPa pressure loading - Complex Weld Model.

Pressure [MPa]	**$\Delta S_{p,k}$ [MPa] (Experimental)**	**$\Delta S_{p,k}$ [MPa] (Numerical)**	**Number of Cycles (Experimental)**	**Kf**	**S_{alt} [MPa] (Experimental)**	**S_{alt} [MPa] (Numerical)**	**Number of Cycles (ASME VIII DIV 2) - Experimental**	**Number of Cycles (Numerical)**
1.6	-	154.51	-	1	-	77.255	-	99900
				2	-	154.51	-	99900
				3	-	231.76	-	31380
				4	-	309.02	-	6393
				5	-	386.27	-	1741
				5.9	-	455.80	-	0
				6.2	-	478.98	-	0

Source: Author (2021)

Table I 6 - Fatigue strength reduction factor (kf) effect in the lifetime of the plates for 0.8 MPa pressure loading - Simple Weld Model.

Pressure [MPa]	**$\Delta S_{p,k}$ [MPa] (Experimental)**	**$\Delta S_{p,k}$ [MPa] (Numerical)**	**Number of Cycles (Experimental)**	**Kf**	**S_{alt} [MPa] (Experimental)**	**S_{alt} [MPa] (Numerical)**	**Number of Cycles (ASME VIII DIV 2) - Experimental**	**Number of Cycles (Numerical)**
0.8	-	83.17	-	1	-	41.58	-	99900
				2	-	83.17	-	99900
				3	-	124.75	-	99900
				4	-	166.34	-	99900
				5	-	207.92	-	69754
				5.9	-	245.35	-	27257
				6.2	-	257.82	-	19317

Source: Author (2021)

Table I 7 - Fatigue strength reduction factor (kf) effect in the lifetime of the plates for 1 MPa pressure loading - Simple Weld Model.

Pressure [MPa]	**$\Delta S_{p,k}$ [MPa] (Experimental)**	**$\Delta S_{p,k}$ [MPa] (Numerical)**	**Number of Cycles (Experimental)**	**Kf**	**S_{alt} [MPa] (Experimental)**	**S_{alt} [MPa] (Numerical)**	**Number of Cycles (ASME VIII DIV 2) - Experimental**	**Number of Cycles (Numerical)**
1	114.18	101.11	14059	1	57.09	52.32	1000000	99900
				2	114.18	104.65	1000000	99900
				3	171.27	156.97	99900	99900
				4	228.02	209.30	55933	80157
				5	-	252.77	-	22140
				5.9	336.83	308.71	13509	8636
				6.2	353.95	324.41	10825	6057

Source: Author (2021)

Table I 8 - Fatigue strength reduction factor (kf) effect in the lifetime of the plates for 1.2 MPa pressure loading - Simple Weld Model.

Pressure [MPa]	**$\Delta S_{p,k}$ [MPa] (Experimental)**	**$\Delta S_{p,k}$ [MPa] (Numerical)**	**Number of Cycles (Experimental)**	**Kf**	**S_{alt} [MPa] (Experimental)**	**S_{alt} [MPa] (Numerical)**	**Number of Cycles (ASME VIII DIV 2) - Experimental**	**Number of Cycles (Numerical)**
1.2	138.47	117.93	8562	1	69.235	58.96	1000000	99900
				2	138.47	117.93	579875	99900
				3	207.705	176.93	79659	99900
				4	276.94	235.86	26860	32160
				5	-	294.83	-	9774
				5.9	408.48	347.89	13509	3447
				6.2	428.26	365.58	5594	2446

Source: Author (2021)

Table I 9 - Fatigue strength reduction factor (kf) effect in the lifetime of the plates for 1.4 MPa pressure loading - Simple Weld Model.

Pressure [MPa]	**$\Delta S_{p,k}$ [MPa] (Experimental)**	**$\Delta S_{p,k}$ [MPa] (Numerical)**	**Number of Cycles (Experimental)**	**Kf**	**S_{alt} [MPa] (Experimental)**	**S_{alt} [MPa] (Numerical)**	**Number of Cycles (ASME VIII DIV 2) - Experimental**	**Number of Cycles (Numerical)**
1.4	163.84	133.82	3167	1	81.92	69.30	1000000	99900
				2	163.84	138.60	228564	99900
				3	245.84	207.84	42353	75832
				4	327.68	277.20	14821	15218
				5	-	334.55	-	4197
				5.9	483.328	408.87	7014	1620
				6.2	507.9	429.66	3122	1145

Source: Author (2021)

Table I 10 - Fatigue strength reduction factor (kf) effect in the lifetime of the plates for 1.6 MPa pressure loading - Simple Weld Model.

Pressure [MPa]	**$\Delta S_{p,k}$ [MPa] (Experimental)**	**$\Delta S_{p,k}$ [MPa] (Numerical)**	**Number of Cycles (Experimental)**	**Kf**	**S_{alt} [MPa] (Experimental)**	**S_{alt} [MPa] (Numerical)**	**Number of Cycles (ASME VIII DIV 2) - Experimental**	**Number of Cycles (Numerical)**
1,6	-	149.13	-	1	-	74.565	-	99900
				2	-	149.13	-	99900
				3	-	223.69	-	39157
				4	-	298.26	-	7851
				5	-	372.83	-	2171
				5.9	-	439.93	-	0
				6.2	-	462.30	-	0

Source: Author (2021)

APPENDIX II - GOODMAN

Table II 11 - Fatigue strength reduction factor (kf) effect in the lifetime of the plates for 0.8 MPa pressure loading - Complex Weld Model.

Pressure [MPa]	**$\Delta S_{p,k}$ [MPa] (Experimental)**	**$\Delta S_{p,k}$ [MPa] (Numerical)**	**Number of Cycles (Experimental)**	**Kf**	**S_{alt} [MPa] (Experimental)**	**S_{alt} [MPa] (Numerical)**	**Number of Cycles (ASME VIII DIV 2) - Experimental**	**Number of Cycles (Numerical)**
0.8	-	86.29	-	1	-	41.15	-	99900
				2	-	82.29	-	99900
				3	-	123.44	-	99900
				4	-	164.58	-	99900
				5	-	215.72	-	34521
				5.9	-	242.76	-	13443
				6.2	-	255.10	-	9501

Source: Author (2021)

Table II 2 - Fatigue strength reduction factor (kf) effect in the lifetime of the plates for 1.0 MPa pressure loading - Complex Weld Model.

Pressure [MPa]	**$\Delta S_{p,k}$ [MPa] (Experimental)**	**$\Delta S_{p,k}$ [MPa] (Numerical)**	**Number of Cycles (Experimental)**	**Kf**	**S_{alt} [MPa] (Experimental)**	**S_{alt} [MPa] (Numerical)**	**Number of Cycles (ASME VIII DIV 2) - Experimental**	**Number of Cycles (Numerical)**
1.0	114.18	104.65	14059.00	1	57.09	52.33	1000000	99900
				2	114.18	104.65	1000000	99900
				3	171.27	156.98	182420	99900
				4	228.02	209.30	55933	36338
				5	-	261.63	-	9972
				5.9	336.83	308.72	13509	3898
				6.2	353.95	324.42	10825	2746

Source: Author (2021)

Table II 3 - Fatigue strength reduction factor (kf) effect in the lifetime of the plates for 1.2 MPa pressure loading - Complex Weld Model.

Pressure [MPa]	**$\Delta S_{p,k}$ [MPa] (Experimental)**	**$\Delta S_{p,k}$ [MPa] (Numerical)**	**Number of Cycles (Experimental)**	**Kf**	**S_{alt} [MPa] (Experimental)**	**S_{alt} [MPa] (Numerical)**	**Number of Cycles (ASME VIII DIV 2) - Experimental**	**Number of Cycles (Numerical)**
1.2	138.47	122.04	8562.0	1	69.24	61.02	1000000	99900
				2	138.47	122.04	579875	99900
				3	207.71	183.06	79659	66047
				4	276.94	244.08	26860	13178
				5	-	305.10	-	3648
				5.9	408.48	360.02	13509	1427
				6.2	428.26	389.32	5594	1009

Source: Author (2021)

Table II 4 - Fatigue strength reduction factor (kf) effect in the lifetime of the plates for 1.4 MPa pressure loading - Complex Weld Model.

Pressure [MPa]	**$\Delta S_{p,k}$ [MPa] (Experimental)**	**$\Delta S_{p,k}$ [MPa] (Numerical)**	**Number of Cycles (Experimental)**	**Kf**	**S_{alt} [MPa] (Experimental)**	**S_{alt} [MPa] (Numerical)**	**Number of Cycles (ASME VIII DIV 2) - Experimental**	**Number of Cycles (Numerical)**
1.4	163.84	138.60	3167.00	1	81.92	69.30	1000000	99900
				2	163.84	138.60	228564	99900
				3	245.84	207.84	42353	27898
				4	327.68	277.20	14821	5657
				5	-	346.50	-	1554
				5.9	483.33	408.87	7014	0
				6.2	507.90	429.66	3122	0

Source: Author (2021)

Table II 5 - Fatigue strength reduction factor (kf) effect in the lifetime of the plates for 1.6 MPa pressure loading - Complex Weld Model.

Pressure [MPa]	**$\Delta S_{p,k}$ [MPa] (Experimental)**	**$\Delta S_{p,k}$ [MPa] (Numerical)**	**Number of Cycles (Experimental)**	**Kf**	**S_{alt} [MPa] (Experimental)**	**S_{alt} [MPa] (Numerical)**	**Number of Cycles (ASME VIII DIV 2) - Experimental**	**Number of Cycles (Numerical)**
1.6	-	154.51	-	1	-	77.26	-	99900
				2	-	154.51	-	99900
				3	-	231.77	-	13453
				4	-	309.02	-	2714
				5	-	386.28	-	0
				5.9	-	455.80	-	0
				6.2	-	478.98	-	0

Source: Author (2021)

Table II 6 - Fatigue strength reduction factor (kf) effect in the lifetime of the plates for 0.8 MPa pressure loading – Simple Weld Model.

Pressure [MPa]	**$\Delta S_{p,k}$ [MPa] (Experimental)**	**$\Delta S_{p,k}$ [MPa] (Numerical)**	**Number of Cycles (Experimental)**	**Kf**	**S_{alt} [MPa] (Experimental)**	**S_{alt} [MPa] (Numerical)**	**Number of Cycles (ASME VIII DIV 2) - Experimental**	**Number of Cycles (Numerical)**
0.8	-	83.17	-	1	-	41.59	-	99900
				2	-	83.17	-	99900
				3	-	124.76	-	99900
				4	-	166.34	-	99900
				5	-	207.93	-	43258
				5.9	-	245.35	-	16944
				6.2	-	257.83	-	11872

Source: Author (2021)

Table II 7 - Fatigue strength reduction factor (kf) effect in the lifetime of the plates for 1.0 MPa pressure loading - Simple Weld Model.

Pressure [MPa]	**$\Delta S_{p,k}$ [MPa] (Experimental)**	**$\Delta S_{p,k}$ [MPa] (Numerical)**	**Number of Cycles (Experimental)**	**Kf**	**S_{alt} [MPa] (Experimental)**	**S_{alt} [MPa] (Numerical)**	**Number of Cycles (ASME VIII DIV 2) - Experimental**	**Number of Cycles (Numerical)**
1.0	114.18	101.11	14059.00	1	57.09	52.33	1000000	99900
				2	114.18	104.65	1000000	99900
				3	171.27	156.98	182420	99900
				4	228.02	209.30	55933	45526
				5	-	252.78	-	12382
				5.9	336.83	308.72	13509	4901
				6.2	353.95	324.42	10825	3414

Source: Author (2021)

Table II 8 - Fatigue strength reduction factor (kf) effect in the lifetime of the plates for 1.2 MPa pressure loading - Simple Weld Model.

Pressure [MPa]	**$\Delta S_{p,k}$ [MPa] (Experimental)**	**$\Delta S_{p,k}$ [MPa] (Numerical)**	**Number of Cycles (Experimental)**	**Kf**	**S_{alt} [MPa] (Experimental)**	**S_{alt} [MPa] (Numerical)**	**Number of Cycles (ASME VIII DIV 2) - Experimental**	**Number of Cycles (Numerical)**
1.2	138.47	117.93	8562	1	69.24	58.97	1000000	99900
				2	138.47	117.93	579875	99900
				3	207.71	176.93	79659	82458
				4	276.94	235.86	26860	16649
				5	-	294.83	-	4568
				5.9	408.48	347.89	13509	1778
				6.2	428.26	365.58	5594	1257

Source: Author (2021)

Table II 9 - Fatigue strength reduction factor (kf) effect in the lifetime of the plates for 1.4 MPa pressure loading - Simple Weld Model.

Pressure [MPa]	**$\Delta S_{p,k}$ [MPa] (Experimental)**	**$\Delta S_{p,k}$ [MPa] (Numerical)**	**Number of Cycles (Experimental)**	**Kf**	**S_{alt} [MPa] (Experimental)**	**S_{alt} [MPa] (Numerical)**	**Number of Cycles (ASME VIII DIV 2) - Experimental**	**Number of Cycles (Numerical)**
1.4	163.84	133.82	3167.00	1	81.92	69.30	1000000	99900
				2	163.84	138.60	228564	99900
				3	245.84	207.84	42353	75832
				4	327.68	277.20	14821	15218
				5	-	334.55	-	4197
				5.9	483.33	408.87	7014	1619
				6.2	507.90	429.66	3122	1145

Source: Author (2021)

Table II - Fatigue strength reduction factor (kf) effect in the lifetime of the plates for 1.0 MPa pressure loading - Simple Weld Model.

Pressure [MPa]	**$\Delta S_{p,k}$ [MPa] (Experimental)**	**$\Delta S_{p,k}$ [MPa] (Numerical)**	**Number of Cycles (Experimental)**	**Kf**	**S_{alt} [MPa] (Experimental)**	**S_{alt} [MPa] (Numerical)**	**Number of Cycles (ASME VIII DIV 2) - Experimental**	**Number of Cycles (Numerical)**
1.6	-	149.13	-	1	-	74.57	-	99900
				2	-	149.13	-	99900
				3	-	223.70	-	16999
				4	-	298.26	-	3427
				5	-	372.83	-	0
				5.9	-	439.93	-	0
				6.2	-	462.30	-	0

Source: Author (2021)

Table II 2 - Fatigue strength reduction factor (kf) effect in the lifetime of the plates for 1.0 MPa pressure loading - Complex Weld Model.

Pressure [MPa]	**$\Delta S_{p,k}$ [MPa] (Experimental)**	**$\Delta S_{p,k}$ [MPa] (Numerical)**	**Number of Cycles (Experimental)**	**Kf**	**S_{alt} [MPa] (Experimental)**	**S_{alt} [MPa] (Numerical)**	**Number of Cycles (ASME VIII DIV 2) - Experimental**	**Number of Cycles (Numerical)**
1.0	114.18	104.65	14059.00	1	57.09	52.33	1000000	99900
				2	114.18	104.65	1000000	99900
				3	171.27	156.98	182420	99900
				4	228.02	209.30	55933	36338
				5	-	261.63	-	9972
				5.9	336.83	308.72	13509	3898
				6.2	353.95	324.42	10825	2746

Source: Author (2021)

APPENDIX III - SODERBERG

Table III 12 - Fatigue strength reduction factor (kf) effect in the lifetime of the plates for 0.8 MPa pressure loading - Complex Weld Model.

Pressure [MPa]	**$\Delta S_{p,k}$ [MPa] (Experimental)**	**$\Delta S_{p,k}$ [MPa] (Numerical)**	**Number of Cycles (Experimental)**	**Kf**	**S_{alt} [MPa] (Experimental)**	**S_{alt} [MPa] (Numerical)**	**Number of Cycles (ASME VIII DIV 2) - Experimental**	**Number of Cycles (Numerical)**
0.8	-	86.29	-	1	-	41.15	-	99900
				2	-	82.29	-	99900
				3	-	123.44	-	99900
				4	-	164.58	-	39172
				5	-	215.72	-	10791
				5.9	-	242.76	-	4244
				6.2	-	255.10	-	2981

Source: Author (2021)

Table III 2 - Fatigue strength reduction factor (kf) effect in the lifetime of the plates for 1.0 MPa pressure loading - Complex Weld Model.

Pressure [MPa]	**$\Delta S_{p,k}$ [MPa] (Experimental)**	**$\Delta S_{p,k}$ [MPa] (Numerical)**	**Number of Cycles (Experimental)**	**Kf**	**S_{alt} [MPa] (Experimental)**	**S_{alt} [MPa] (Numerical)**	**Number of Cycles (ASME VIII DIV 2) - Experimental**	**Number of Cycles (Numerical)**
1.0	114.18	104.65	14059.00	1	57.09	52.33	1000000	99900
				2	114.18	104.65	1000000	99900
				3	171.27	156.98	182420	41192
				4	228.02	209.30	55933	8361
				5	-	261.63	-	2300
				5.9	336.83	308.72	13509	0
				6.2	353.95	324.42	10825	0

Source: Author (2021)

Table III 3 - Fatigue strength reduction factor (kf) effect in the lifetime of the plates for 1.2 MPa pressure loading - Complex Weld Model.

Pressure [MPa]	**$\Delta S_{p,k}$ [MPa] (Experimental)**	**$\Delta S_{p,k}$ [MPa] (Numerical)**	**Number of Cycles (Experimental)**	**Kf**	**S_{alt} [MPa] (Experimental)**	**S_{alt} [MPa] (Numerical)**	**Number of Cycles (ASME VIII DIV 2) - Experimental**	**Number of Cycles (Numerical)**
1.2	138.47	122.04	8562.00	1	69.24	61.02	1000000	99900
				2	138.47	122.04	579875	99900
				3	207.71	183.06	79659	10954
				4	276.94	244.08	26860	2207
				5	-	305.10	-	0
				5.9	408.48	360.02	13509	0
				6.2	428.26	389.32	5594	0

Source: Author (2021)

Table III 4 - Fatigue strength reduction factor (kf) effect in the lifetime of the plates for 1,4 MPa pressure loading - Complex Weld Model.

Pressure [MPa]	**$\Delta S_{p,k}$ [MPa] (Experimental)**	**$\Delta S_{p,k}$ [MPa] (Numerical)**	**Number of Cycles (Experimental)**	**Kf**	**S_{alt} [MPa] (Experimental)**	**S_{alt} [MPa] (Numerical)**	**Number of Cycles (ASME VIII DIV 2) - Experimental**	**Number of Cycles (Numerical)**
1.4	163.84	138.60	3167.00	1	81.92	69.30	1000000	99900
				2	163.84	138.60	228564	37201
				3	245.84	207.84	42353	3323
				4	327.68	277.20	14821	0
				5	-	346.50	-	0
				5.9	483.33	408.87	7014	0
				6.2	507.90	429.66	3122	0

Source: Author (2021)

Table III 5 - Fatigue strength reduction factor (kf) effect in the lifetime of the plates for 1.6 MPa pressure loading - Complex Weld Model.

Pressure [MPa]	**$\Delta S_{p,k}$ [MPa] (Experimental)**	**$\Delta S_{p,k}$ [MPa] (Numerical)**	**Number of Cycles (Experimental)**	**Kf**	**S_{alt} [MPa] (Experimental)**	**S_{alt} [MPa] (Numerical)**	**Number of Cycles (ASME VIII DIV 2) - Experimental**	**Number of Cycles (Numerical)**
1.6	-	154.51	-	1	-	77.26	-	99900
				2	-	154.51	-	12178
				3	-	231.77	-	1098
				4	-	309.02	-	0
				5	-	386.28	-	0
				5.9	-	455.80	-	0
				6.2	-	478.98	-	0

Source: Author (2021)

Table III 6 - Fatigue strength reduction factor (kf) effect in the lifetime of the plates for 0.8 MPa pressure loading - Simple Weld Model.

Pressure [MPa]	**$\Delta S_{p,k}$ [MPa] (Experimental)**	**$\Delta S_{p,k}$ [MPa] (Numerical)**	**Number of Cycles (Experimental)**	**Kf**	**S_{alt} [MPa] (Experimental)**	**S_{alt} [MPa] (Numerical)**	**Number of Cycles (ASME VIII DIV 2) - Experimental**	**Number of Cycles (Numerical)**
0.8	-	83.17	-	1	-	41.59	-	99900
				2	-	83.17	-	99900
				3	-	124.76	-	99900
				4	-	166.34	-	51879
				5	-	207.93	-	14374
				5.9	-	245.35	-	5616
				6.2	-	257.83	-	3946

Source: Author (2021)

Table III 7 - Fatigue strength reduction factor (kf) effect in the lifetime of the plates for 1.0 MPa pressure loading - Simple Weld Model.

Pressure [MPa]	**$\Delta S_{p,k}$ [MPa] (Experimental)**	**$\Delta S_{p,k}$ [MPa] (Numerical)**	**Number of Cycles (Experimental)**	**Kf**	**S_{alt} [MPa] (Experimental)**	**S_{alt} [MPa] (Numerical)**	**Number of Cycles (ASME VIII DIV 2) - Experimental**	**Number of Cycles (Numerical)**
1.0	114.18	101.11	14059.00	1	57.09	52.33	1000000	99900
				2	114.18	104.65	1000000	99900
				3	171.27	156.98	182420	54698
				4	228.02	209.30	55933	11121
				5	-	252.78	-	3063
				5.9	336.83	308.72	13509	1196
				6.2	353.95	324.42	10825	0

Source: Author (2021)

Table III 8 - Fatigue strength reduction factor (kf) effect in the lifetime of the plates for 1.2 MPa pressure loading - Simple Weld Model.

Pressure [MPa]	**$\Delta S_{p,k}$ [MPa] (Experimental)**	**$\Delta S_{p,k}$ [MPa] (Numerical)**	**Number of Cycles (Experimental)**	**Kf**	**S_{alt} [MPa] (Experimental)**	**S_{alt} [MPa] (Numerical)**	**Number of Cycles (ASME VIII DIV 2) - Experimental**	**Number of Cycles (Numerical)**
1.2	138.47	117.93	8562	1	69.24	58.97	1000000	99900
				2	138.47	117.93	579875	99900
				3	207.71	176.93	79659	14942
				4	276.94	235.86	26860	2993
				5	-	294.83	-	0
				5.9	408.48	347.89	13509	0
				6.2	428.26	365.58	5594	0

Source: Author (2021)

Table III 9 - Fatigue strength reduction factor (kf) effect in the lifetime of the plates for 1.4 MPa pressure loading - Simple Weld Model.

Pressure [MPa]	**$\Delta S_{p,k}$ [MPa] (Experimental)**	**$\Delta S_{p,k}$ [MPa] (Numerical)**	**Number of Cycles (Experimental)**	**Kf**	**S_{alt} [MPa] (Experimental)**	**S_{alt} [MPa] (Numerical)**	**Number of Cycles (ASME VIII DIV 2) - Experimental**	**Number of Cycles (Numerical)**
1.4	163.84	133.82	3167.00	1	81.92	69.30	1000000	99900
				2	163.84	138.60	228564	51834
				3	245.84	207.84	42353	4666
				4	327.68	277.20	14821	0
				5	-	334.55	-	0
				5.9	483.33	408.87	7014	0
				6.2	507.90	429.66	3122	0

Source: Author (2021)

Table III 10 - Fatigue strength reduction factor (kf) effect in the lifetime of the plates for 1.6 MPa pressure loading - Simple Weld Model.

Pressure [MPa]	**$\Delta S_{p,k}$ [MPa] (Experimental)**	**$\Delta S_{p,k}$ [MPa] (Numerical)**	**Number of Cycles (Experimental)**	**Kf**	**S_{alt} [MPa] (Experimental)**	**S_{alt} [MPa] (Numerical)**	**Number of Cycles (ASME VIII DIV 2) - Experimental**	**Number of Cycles (Numerical)**
1.6	-	149.13	-	1	-	74.57	-	99900
				2	-	149.13	-	17735
				3	-	223.70	-	1589
				4	-	298.26	-	0
				5	-	372.83	-	0
				5.9	-	439.93	-	0
				6.2	-	462.30	-	0

Source: Author (2021)